PPS
Perspective
www.rsc.org/pps

Electronic states and transitions in C_{60} and C_{70} fullerenes

Giorgio Orlandi *[a] **and Fabrizia Negri** *[b]

[a] *Dipartimento di Chimica "G. Ciamician", Via F. Selmi, 2, I-40126 Bologna, Italy. E-mail: gorlandi@ciam.unibo.it; Fax: +39 051 2099456; Tel: +39 051 209 9472*
[b] *Dipartimento di Chimica "G. Ciamician", Via F. Selmi, 2, I-40126 Bologna, Italy. E-mail: fabry@ciam.unibo.it; Fax: +39 051 2099456; Tel: +39 051 209 9471*

Received 4th January 2002, Accepted 14th March 2002
First published as an Advance Article on the web 3rd April 2002

A review of the most relevant aspects of fullerene electronic structure and spectroscopy is presented. Experimental data and their interpretation based on computational results are discussed both for fullerene C_{60} and C_{70}, with particular attention to the properties of the isolated molecule. Concerning singlet state spectroscopy, it is shown that because of its high symmetry, only dipole-forbidden electronic states are found in the low excitation energy region of C_{60}. Conversely, the lowering of symmetry in C_{70} leads to several complications in its electronic structure and spectroscopy, due to the presence of weakly allowed transitions in the low excitation energy region. A slightly less congested distribution of low lying excited states characterizes the triplet manifold of the fullerenes. It is concluded that while C_{60} is important in aiding understanding of the main features in electronic spectroscopy of fullerenes, such as the presence of strong absorptions in the high energy range, its spectra are deeply influenced by its high symmetry and are very peculiar. On the other hand, C_{70}, with its lower symmetry and more complex spectra, represents a more realistic model for the intricate details of the electronic structure and electronic spectroscopy of larger and smaller fullerenes and their derivatives, which are generally characterized by lower symmetry compared to C_{60}.

1 Introduction

Since their discovery in the middle 1980s[1] fullerenes have attracted a great deal of interest because of their unique structure and properties. It was soon realized that C_{60}, because of its high symmetry and stability, was also unique among the experimentally available fullerenes. Indeed, moving from C_{60} to C_{70}, the second most abundant fullerene, the symmetry decreases from I_h to D_{5h}, and much lower symmetry characterizes most fullerene derivatives. Among the properties of fullerenes that can be related to their electronic structure and their symmetry, the optical properties are of particular relevance in view of the potential applications that might be based on them, such as the production of fullerene-based optical limiters.[2]

In this contribution we review the optical properties of the two most abundant fullerenes, C_{60} and C_{70} (see Fig. 1), by focussing on electronic spectroscopy studies carried out in solution, noble gas matrices or in the gas phase, in other words in conditions where the properties of approximately isolated molecules can be monitored. These spectroscopic studies represent an important source of information about the effect of intra-molecular couplings, although the interactions with the solvent will also cause significant perturbations that appear

Giorgio Orlandi graduated in Chemistry at the University of Padua in 1964. In 1970/1971 he worked for one year with W. Siebrand at the National Research Council of Canada, Ottawa, and, in 1978, he was at the Max-Planck-Institut für Biophysikalische Chemie, Göttingen, as a von Humboldt fellow. In 1969 he became Research Officer at the Institute of Photochemistry and Radiation Chemistry of the National Research Council of Italy and in 1981 he joined the University of Bologna as Professor of Physical Chemistry. His research interests include theoretical chemistry, vibrational and electronic spectroscopy, photophysical and photochemical properties of molecular systems.

Fabrizia Negri received her PhD in Chemical Physics, in 1991, from the University of Bologna. After the PhD she spent two years as a post-doctorate research assistant at the National Research Council of Canada, Ottawa, where she worked with W. Siebrand and M. Zgierski on the spectroscopy of several conjugated molecules and collaborated with EPR spectroscopists on the study of fullerene derivatives. She then returned to Bologna where she is now Associate Professor in Chemical Physics. In 1997 she was awarded the Federchimica Prize. Her major scientific interests include, currently, the modeling of large polycyclic aromatic hydrocarbons, their three-dimensional dendrimeric precursors and their lithium and hydrogen storage capacities.

DOI: 10.1039/b200178k

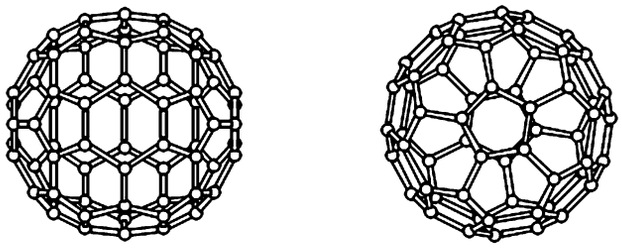

Fig. 1 The two most abundant fullerenes C_{60} (right) and C_{70} (left)

in the spectra. On the other hand, these spectroscopic data are (the only data) directly comparable with the results of quantum-chemical computational studies carried out on isolated fullerene molecules.

An important aspect that we wish to emphasize is the fact that the constant feedback between experiment and theory has been fundamental in obtaining a convincing identification of the lowest excited states of fullerenes.

Indeed, the main problem with these carbon clusters is the extremely high density of electronic states already found at the onset of the absorption spectrum. From an experiemental point of view this implies that high resolution spectra are required to properly distinguish the electronic and vibronic structure. On the other hand, such high density of electronic states pushes to their limit the prediction capabilities of quantum-chemical calculations, since electronic states cannot be predicted with the accuracy of tens of cm^{-1}, for systems as large as fullerenes. It follows that simple lists of predicted electronic excited states are of little use in interpreting the observed vibronic and electronic structure, whilst the fundamental contribution is provided by the modeling of vibronic intensities associated with the predicted electronic states that fall in the energy region explored experimentally. It is only the combination of the two sources of information, detailed experimental vibronic structure and accurate modeling of vibronic intensities, that has led to a satisfactory assignment of the electronic spectra of fullerenes.

In the following we will start, first, with an account of the spectroscopy of C_{60}, the most abundant fullerene, and we will review the excited states and spectroscopic charecteristics of C_{70} in the second part of the paper. All the computational details and the principles governing allowed and induced vibronic transitions are summarized in the following section.

2 Computational methods and modeling of vibronic intensities

From the computational point of view, these large systems still represent a challenge, especially when considering the study of excited electronic states and their properties. A knowledge, as precise as possible, of their energy order is necessary to analyse and model the vibronic structure observed in the electronic spectra of fullerenes. In this sense, quantum-chemical calculations based on semiempirical hamiltonians have offered the only accessible way to predict a large number of electronic excited states along with the vibronic and spin–orbit interactions required to model the vibronic structure associated with the electronic transitions.

To analyze the vibronic structure of the electronic spectra of fullerenes, quantum chemical calculations of equilibrium structures and vibrational force fields were carried out with the help of the QCFF/PI (quantum consistent force field for π electrons) semiempirical method.[3]

Electronic excitation energies and transition dipole moments were computed with the CNDO/S (complete neglect of differential overlap for spectroscopy) hamiltonian,[4] combined with configuration interaction (CI) calculations that included single excited configurations (SECs) or single and double excited configurations (DECs).

2.1 Herzberg–Teller intensity borrowing

Vibronically induced intensities can be obtained by differentiating transition dipole-moments with respect to vibrational normal coordinates, as described in detail in ref. 5

2.2 Franck–Condon and Jahn–Teller activity

The activity of Franck–Condon (FC) active vibrations (totally-symmetric (TS) vibrations) can be estimated by computing the associated γ parameters along the lines described in ref. 6. The γ parameters were generally computed with the QCFF/PI method.[3] The same procedure can be followed to estimate the Jahn–Teller (JT) activity of JT active vibrations (a specific set of non-totally-symmetric (NTS) vibrations), in the limit of strong coupling which leads to a static JT deformation.[6,7]

The intensity ratio between the vibronic band corresponding to the fundamental of the i-th mode, and the origin band, is proportional to the γ_i parameter.

2.3 Intensity borrowing in phosphorescence spectra

The calculation of the $T_1 \longrightarrow S_0$ transition dipole moment (M) requires the inclusion of the spin–orbit (SO) perturbation.

The spin–orbit couplings $H_{SO}(S_k,T_j^a)$ between every singlet state S_k and the three components $a = x, y, z$ of every triplet state T_j resulting from CI calculations, were evaluated in the one-electron approximation, according to the approach of ref. 8.

The spin–orbit induced transition dipole moment was computed according to first order perturbation theory.

$$M(S_0, T_1) = \sum_k M(S_0, S_k) \times \frac{H_{SO}(S_k, T_1)}{(E_1 - E_k)} + \sum_m M(T_m, T_1) \times \frac{H_{SO}(S_0, T_m)}{(E_0 - E_m)}$$

In the expression above, k and m run over the full space of singlet and triplet states considered in the CI calculations.

Similarly to benzene, the $T_1 \longrightarrow S_0$ transition dipole moment is zero by symmetry both for C_{60} and C_{70}. This implies that the vibronic structure of the phosphorescence spectra is dominated by Herzberg–Teller (HT) induced false origins.

Thus, the estimate of the vibronically induced intensities in the phosphorescence spectrum requires additional evaluation of the numerical derivatives of the $M(S_0, T_1)$ transition dipole moment with respect to each normal coordinate which may be active on the basis of symmetry selection rules.

3 C_{60}

The C_{60} molecule contains 60 carbon atoms arranged in 20 six-membered and 12 five-membered rings. The most stable of the 1812 possible isomers of C_{60}, and the only one that is actually observed, follows the isolated pentagons rule,[9] that is, each of its five-membered rings is completely surrounded by hexagons. Consequently, the only form of C_{60} that is observed belongs to the icosahedral (I_h) symmetry group. The CC bonds separating two hexagons are 1.40 Å and have a substantial double bond character while the pentagon CC bonds are 1.46 Å[10] long and have a prevalent single bond character.

3.1 Orbitals

In a simple quantum-chemical description of the electronic structure of C_{60}, based on the molecular orbital approach, each carbon atom contributes with 4 valence orbitals (2s, $2p_x$, $2p_y$, $2p_z$) and thus C_{60} has 120 occupied molecular orbitals (MOs) and 120 unoccupied or virtual MOs. With some approximations (C_{60} is not planar), 60 MOs (30 occupied and 30 virtual) can be considered of π type and the remaining 180 orbitals of

Table 1 Character table of the *I* point group ($I_h = I \times i$)

Irreducible representation	*I*	$12C_5$	$12C_5^2$	$20C_3$	$15C_2$
A	1	1	1	1	1
T_1	3	$(1 + 5^{1/2})/2$	$(1 - 5^{1/2})/2$	0	−1
T_2	3	$(1 - 5^{1/2})/2$	$(1 + 5^{1/2})/2$	0	−1
G	4	−1	−1	1	0
H	5	10	10	−1	1

Table 2 C_{60} molecular orbitals energies (in eV), I_h symmetry labelling and angular momentum quantum number *l*

Symmetry	Energy	Type	*l*-shell	
g_u, t_{2g}	0.6/1.0 [a]	π*	7-k, 8-l	
g_g	−0.2/0.0 [a]	π*	6-i	
h_u, h_g, t_{2u}	−0.7/−1.2 [a]	π*	7-k, 6-i, 5-h	
t_{1g}	−2.3 [a]	π*	6-i	
t_{1u}	−2.69 [b]	π*	5-h	LUMO
h_u	−8.74 [c]	π	5-h	HOMO
g_g, h_g	−10.14 [c]	π	4-g	
g_u, t_{2u},	−10.74/−11.94 [c]	π	3-f	
h_u, h_g	−10.74/−11.94 [c]	σ	9-m, 10-n	

[a] From ref. 11. [b] From ref. 12. [c] From ref. 13.

σ type. In analogy with large aromatic compounds, the highest occupied MOs (HOMOs) and the lowest unoccupied MOs (LUMOs), which determine the lower electronically excited states, are of π type.

The molecular orbitals of C_{60} can be classified according to the I_h irreducible representations. In Table 1 we list the character table for the *I* point group from which the characters of the I_h point group, $I_h = I \times i$, are easily derived. Furthermore, if we consider the icosahedral symmetry as a perturbed spherical symmetry, we can classify approximately the C_{60} MOs according to the angular momentum quantum number *l* of the spherical harmonics. The degeneracies of I_h orbitals are 1 (a_g, a_u), 3 (t_{1u}, t_{1g}, t_{2u}, t_{2g}), 4 (g_u, g_g) and 5 (h_g, h_u). The degeneracies of spherical harmonics are 1 (s), 3 (p), 5 (d), 7 (f), 9 (g), 11 (h), 13 (i) and so on. In the I_h symmetry, s, p and d orbitals transform as a_g, t_{1u} and h_g, respectively. However, f, g, h and i orbitals, with degeneracies higher than 5, split in $g_u + t_{2u}$ (f), $h_g + g_g$ (g), $h_u + t_{1u} + t_{2u}$ (h) and $a_g + t_{1g} + g_g + h_g$ (i), respectively.

The energies of MOs can be obtained by the Hartree–Fock approach and by proper experiments. The energies of occupied MOs were determined by the photoelectron spectroscopy (PES) technique,[11] while the energy of the LUMO was obtained by the PES of the anion[12] and the energies of virtual orbitals were estimated from near-edge X-ray absorption fine structure (NEXAFS).[13] The experimental energies of the MOs relevant to the visible and near UV electronic transitions are reported in Table 2. The negative energies of the t_{1u} LUMO account for the large electron affinity shown by this molecule which can be reduced to the hexa-anion form in solution and can exist in the gas phase as the dianion.[14]

3.2 Electronic states

The electronic ground state of C_{60} is a closed shell and has A_g symmetry. The five lowest excited configurations and the corresponding state symmetries are

HOMO → LUMO	$h_u \rightarrow t_{1u}$	T_{1g}, T_{2g}, G_g, H_g
HOMO – 1 → LUMO	$h_g \rightarrow t_{1u}$	T_{1u}, T_{2u}, G_u, H_u
HOMO → LUMO + 1	$h_u \rightarrow t_{1g}$	T_{1u}, T_{2u}, G_u, H_u
HOMO – 1 → LUMO + 1	$h_g \rightarrow t_{1g}$	T_{1g}, T_{2g}, G_g, H_g
HOMO – 2 → LUMO	$g_g \rightarrow t_{1u}$	T_{2u}, G_u, H_u

The states deriving from the HOMO–LUMO configuration are expected to be the lowest excited states. In the I_h symmetry group, the translation components *x*, *y*, *z* transform according to the T_{1u} irreducible representation and so does the electric dipole moment. Therefore, the electric dipole moment transition between the A_g ground state and an excited state is allowed only for T_{1u} excited states. Transitions from the ground state to states of other symmetries are forbidden and can occur only by means of the activity of suitable non-totally-symmetric vibrations, *via* the HT vibronic coupling mechanism.

The excited states of lower energy, which originate from the HOMO–LUMO excitations, are symmetry forbidden and thus the absorption spectrum is expected to begin on the low energy side with very weak bands. Correspondingly, the emission spectra are expected to show a very small radiative rate constant and a very low emission quantum yield. This picture is indeed confirmed by experiments (*vide infra*).

The electronic states in the visible and near UV can be both of singlet and triplet spin multiplicity which we shall discuss separately.

3.3 Singlet electronic states

A large molecule like C_{60} has an enormous number of electronic excited states. Even a calculation based only on singly excited electronic configurations from 120 occupied and 120 unoccupied MOs leads to 14400 states. Calculations of energies and oscillator strengths of the lower excited states have been performed by several authors,[5,15–17] but in all of them some approximations had to be made because of the size of the molecule. These calculations were based on semiempirical hamiltonians, QCFF/PI, CNDO/S and INDO/S, and on CI treatments limited to about 1000 SECs. Calculations carried out with time dependent density functional theory have also been reported.[18] Comparing the results of the various authors, it appears that calculations of this size can give a realistic description of the lowest electronic states. In a simplified, but meaningful analysis of the electronic spectra of C_{60}, we need to consider only a few of the *ca.* 1000 states that are actually calculated. Accordingly, in Table 3, where CNDO/S results for the lowest singlet states are shown, only a small number of singlet states are listed. Up to the energy of 3 eV all the calculated excited singlet states are reported, while above this energy threshold only the T_{1u} states are listed together with their oscillator strengths. The high values of some oscillator strengths, which include the contributions of the three T_{1u} substates, are related to the large molecular size of fullerenes and to the consequently large values that transition moments can attain. The list ends at the energy of 7 eV, above which experimental information is not available and theoretical results become less reliable. The results presented in Table 3, obtained by two different calculations, are quite similar: this exemplifies the fact that the electronic state calculations provide a consistent picture of singlet excited states of C_{60}. The picture that emerges fits with the experimental results and can be summarized as follows.

(1) The lowest electronic states are the four T_{1g}, T_{2g}, G_g and H_g states, which have also very similar energies. Actually, the lowest three T_{1g}, T_{2g} and G_g states, which are predicted at 2.3 eV, are found to be practically degenerate, within 0.05 eV (400 cm^{-1}) of one another, while the H_g state is predicted to be 0.3 eV above G_g. Slightly above, at 2.77 eV, a T_{2u} state is computed. For all these states the electric dipole moment transition to the ground state is zero by symmetry.

(2) The lowest T_{1u} state is calculated at 3.4 eV, that is, *ca.* 1 eV above the lowest excited singlets. The T_{1u} excited states with larger oscillator strengths are found at 4.3, 5.2 and 5.7 eV. The large energy gap between the lowest energy singlet states and the intensity lending T_{1u} states allows one to describe the intensity borrowing by means of the HT perturbation

Table 3 C_{60} electronic excited state energies (in eV) and transition oscillator strengths (f)

EEL[a]	EEL[b]	Abs.[c]	Abs.[d]	f[d]	Assignment[e]	E; f[f]	E; f[g]
1.55					$1\ ^3T_{2g}$		
1.72							
1.92			1.82–1.97		$1\ ^1T_{2g}$, $1\ ^1T_{1g}$		2.29
2.20	2.24		2.0–2.21		$1\ ^1G_g$		2.34
2.36			2.25–2.32		$1\ ^1H_g$		2.66
2.58			2.36–2.50		$1\ ^1T_{2u}$		2.77
2.74		2.7	2.9–2.93		$1\ ^1H_u$		3.02
3.0	2.98	3.07	2.99–3.02		$1\ ^1G_u$		3.12
3.3			3.04–3.26	0.005	$1\ ^1T_{1u}$	3.4; 0.08	3.4; 0.12
3.4	3.4		3.29–3.46		$2\ ^1T_{1u}$	4.06; 0.41	4.02; 0.54
3.7	3.77	3.77	3.78	0.37	$3\ ^1T_{1u}$	4.38; 2.37	4.28; 2.70
	4.4		4.06–4.35	0.1	$4\ ^1T_{1u}$,	4.7; 0.3	4.64; 0.54
					$5\ ^1T_{1u}$	5.07; —	5.03; 2.94
4.8	4.88	4.8	4.84	2.27	$6\ ^1T_{1u}$	5.24; 7.88	5.20; 5.79
5.5			5.46	0.22	$7\ ^1T_{1u}$	5.54; 1.18	5.51; 0.81
5.8		5.8	5.88	3.09	$8\ ^1T_{1u}$	5.78; 10.7	5.62; 3.21
6.3	6.43		6.36		$9\ ^1T_{1u}$	6.28; —	6.31; 0.42

[a] From ref. 21. [b] From ref. 22. [c] From ref. 19. [d] From ref. 20. [e] From ref. 20 and from calculations of columns 7 and 8. [f] From ref. 17. [g] From ref. 5.

approach, despite the high density of electronic states. In fullerenes of lower symmetry, like C_{70}, forbidden and allowed states will be closer in energy and the interpretation of vibronic spectra is more complicated (see section 4.1.2).

These theoretical results are now compared with the spectroscopic observations.

Information about the distribution of the excited electronic states as a function of energy is provided by various spectroscopic techniques, in particular by absorption spectroscopy[19,20] and by high resolution electron energy loss (HREEL) spectroscopy.[21,22] The latter technique is not subject to the dipole moment selection rule and thus, by tuning the electron beam energy, it can reveal also the dipole forbidden states. However, as discussed above, these states do also appear, albeit weakly, in the conventional absorption spectra *via* the HT mechanism.

The distribution of the C_{60} electronic states down to 200 nm is well illustrated by the classical absorption spectrum observed in *n*-hexane solution at room temperature by Leach and co-workers.[20] This spectrum, shown in Fig. 2, is very similar to

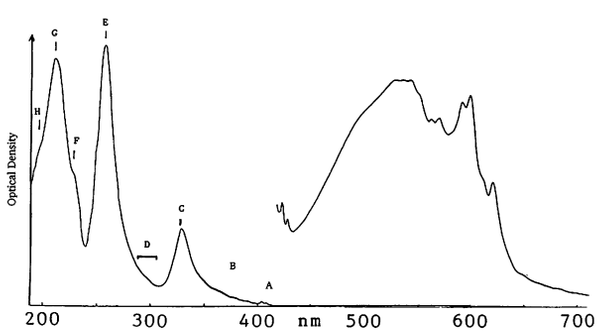

Fig. 2 Room temperature absorption spectrum of C_{60} in *n*-hexane solutions (from ref. 20). A–H indicate bands or shoulders assigned to T_{1u} states (see text). Optical density (absorbance) is in arbitrary units.

the spectra recorded in other matrices (for example in Ar, H_2) and in HREEL spectra.[21,22] The energies of band maxima and of shoulders are reported in Table 3 where their assignment proposed on the basis of quantum chemical calculations is shown.

Considering only the dominant features of these spectra, we can distinguish the following spectral regions.

(1) A strong band region between 200 and 350 nm, containing three intense bands with maxima at 211, 256 and 328 nm, labelled C, E and G, respectively. These bands are associated with the electronic states with the largest oscillator strengths $3T_{1u}$, $6T_{1u}$ and $8T_{1u}$ (see Table 3). Furthermore, shoulders can be identified at 195 (H), 227 (F), and 295 nm (D) associated with the states $9T_{1u}$, $7T_{1u}$ and $4T_{1u}$, and $5T_{1u}$, respectively. The strong bands are about 2500 cm^{-1} full width at half maximum (FWHM) and are structureless. This property may be the result of two factors: the first is the inhomogeneous broadening due to the dilution of the oscillator strength of the intense state, for example our $6T_{1u}$ in the CI of approximately 1000 configurations, among the several T_{1u} states that will result in the same energy range with a larger CI treatment. The second is the homogeneous broadening of each electronic state. With a lifetime of 100 fs (plausible for the high energy excited states), the homogeneous linewidth will be *ca.* 50 cm^{-1}. Actually, several T_{1u} states have been observed with a linewidth of about 50 cm^{-1} or larger.[23–27] The short lifetime of the excited states in the energy range of 200–350 nm, required in order to explain the homogeneous linewidth of 50 cm^{-1}, is compatible with a high density of electronic states which is very likely to lead to crossing of potential energy surfaces or conical intersections.

(2) A spectral region extending from 350 to 430 nm containing weaker bands with most of the intensity generated by transitions to the lowest T_{1u} state. In this region it possible to recognize some vibrational structure associated with each electronic transition. This spectral region has been explored accurately by excitation spectroscopy in a supersonic beam[23] and, recently, in a Ne matrix at 4 K.[27] Several vibrational bands have been observed that can be assigned as JT vibronic bands based on electronic transitions to the $1T_{1u}$ state and to other u states.

(3) Above 430 nm up to 640 nm, one finds a series of very weak bands associated with the low energy g states for which the transition to or from S_0 is symmetry forbidden.[5,6,20] The observed weak bands are due to false origins induced by the HT mechanism and to the combination bands of inducing modes with a_g and h_g JT active modes. Actually, as will be discussed in detail below, most of the vibrational structure in this region is due to false origins.

3.4 Lowest singlet excited states

The fluorescence and visible absorption spectra of fullerene have attracted considerable interest because they provide information about the lowest excited electronic states. As discussed above, the three lowest states of C_{60}, which lie within ~0.05 eV, belong to the T_{2g}, T_{1g} and G_g irreducible representations. This conclusion is supported by quantum chemical calculations,[5,15–17] and by the very weak intensity of the bands appearing on the long wavelength side of the absorption spectra in the *n*-hexane matrix[20] and in the argon matrix.[28] Thus,

Table 4 Computed oscillator strengths (f) of vibronically induced false origins for the $S_0 \longrightarrow 1T_{1g}$, $S_0 \longrightarrow 1T_{2g}$, $S_0 \longrightarrow 1G_g$, $S_0 \longrightarrow 1H_g$ transitions in C_{60}. The size of the CI matrix is 930[a]

				$f \times 10^4$			
Symmetry	n	ν exp./cm^{-1} [b]	ν calc./cm^{-1} [c]	T_{1g}	T_{2g}	G_g	H_g
a_u	1	976	1074	0.0	0.0	0.0	0.0
t_{1u}	1	525	504	0.0	0.0	0.0	18.9
	2	578	605	0.0	0.0	0.0	0.0
	3	1180	1186	4.1	0.0	0.0	2.0
	4	1430	1429	78.5	0.0	0.0	45.1
t_{2u}	1	354	322	0.0	0.0	0.0	0.1
	2	715	632	0.0	0.0	10.5	35.7
	3	1037	985	0.0	0.0	0.0	0.0
	4	1190	1235	0.0	0.0	2.9	0.0
	5	1540	1496	0.0	0.0	0.4	3.9
g_u	1	345	333	0.0	6.0	5.2	12.9
	2	757	748	0.0	5.2	8.1	1.8
	3	776	755	0.0	2.4	34.7	0.4
	4	963	992	0.0	18.1	0.0	0.0
	5	1315	1348	0.0	0.4	16.1	7.7
	6	1410	1478	0.0	87.3	0.0	28.0
h_u	1	403	379	5.9	22.1	0.0	0.5
	2	525	491	0.3	0.6	23.4	0.7
	3	667	666	1.1	0.8	9.4	6.6
	4	738	745	4.2	0.0	95.4	13.3
	5	1215	1224	5.3	4.5	0.2	2.9
	6	1342	1380	0.0	0.1	0.9	0.9
	7	1566	1563	23.3	86.4	1.1	0.5

[a] From ref. 6. [b] From ref. 31 with a few reassignments proposed in ref. 29. [c] From ref. 30.

their transitions to and from the ground state are symmetry forbidden and the observed vibronic bands reflect the effects of the HT mechanism, of the FC activity and, possibly, of the matrix perturbations. The dominant features of these spectra are due to the *ungerade* modes of proper symmetry that mix the electronic states involved in the forbidden transitions (A_g and G_g, T_{1g}, T_{2g}, H_g) with electronic states of different parity such as to render the transition allowed.

The HT active modes for the transition to and from the different g-type electronic states are:

T_{1g}: a_u, t_{1u}, h_u
T_{2g}: g_u, h_u
G_g: t_{2u}, g_u, h_u
H_g: t_{1u}, t_{2u}, g_u, h_u

The relative HT activity of the observed modes in the spectra is an indication of the electronic symmetry of the states participating in a forbidden electronic transition and this is an important criterion to be used in vibronic analyses of C_{60} spectra. In order to identify the vibrational modes responsible for the observed false origin bands, mode activities have been calculated for the three lowest excited electronic states, namely T_{2g}, T_{1g} and G_g[5,6,29] and for the lowest T_{2u} and H_g states[6] that, according to calculations, are 3420 and 2560 cm^{-1} above G_g. The computed oscillator strengths for each HT false origin are presented in Table 4. The calculations have been made on the basis of ground state vibrational modes and frequencies and thus are strictly valid for fluorescence transitions. Since a one-electron promotion in a large molecule like C_{60}, containing 240 valence electrons, causes small changes in the overall electronic density and, therefore, in the force field, the ground state vibrational coordinates are a good basis also for the analysis of absorption spectra. The ground state normal coordinates were calculated by the QCFF/PI hamiltonian[30] and the experimental vibrational frequencies have been taken from Schettino *et al.*,[31] with some further revisions by Negri and Orlandi[30] and Sassara *et al.*[6]

The γ_i parameters that measure the ability of the a_g and h_g modes to form combination bands and progressions, were also estimated on the basis of QCFF/PI calculations.[5,6] It was found that the $h_g(1)$ mode, at 266 cm^{-1}, was the most active, followed by the $a_g(2)$ mode, at 1468 cm^{-1}.

3.4.1 Fluorescence spectra. Fluorescence spectra provide important information about the nature of the lowest excited singlet state that is responsible for the emission and the photophysical properties of C_{60}. The first fluorescence spectrum, measured in a methylcyclohexane matrix at 77 K,[30] had a moderate resolution and showed the strongest band to be shifted by 1455 cm^{-1} from the origin. This led Negri *et al.*,[5] on the basis of the calculated vibronic intensities of Table 4, to assign the state S_1 to the symmetry type T_{1g}. Subsequently, several high resolution fluorescence studies were performed in very low temperature matrices. Van den Heuvel *et al.*[33] measured the C_{60} fluorescence in decalin (decahydronaphthalene)–cyclohexane (DC) glassy matrices at low temperature (1.2 K), and by analyzing the rich vibrational structure in terms of the computed intensities of false origins concluded that the emitting state, S_1, is of dominant T_{1g} character, but appreciably contaminated by the G_g character of the nearby state. Hung *et al.*[34] observed the fluorescence of C_{60} in solid Ne at 5 K, as well as the fluorescence excitation spectra and proposed that the first excited singlet state is $1T_{2g}$ and the second excited singlet $1T_{1g}$. Following a reanalysis of the above fluorescence spectra and of the fluorescence excitation spectra of Groenen and co-workers,[33] Negri *et al.*[29] supported the proposal that S_1 is of dominant T_{1g} character, but is appreciably contaminated by the G_g character and, furthermore, suggested that the state of dominant G_g character is *ca.* 110 cm^{-1} above S_1. Sassara *et al.*[6,35] recorded the fluorescence and the excitation spectra of C_{60} in Ne and Ar matrices at 4 K. Their spectral assignments, based on the calculated vibronic transition intensities, obtained satisfactory agreement between the experimental and simulated spectra. Since the fluorescence spectrum contains false origins that are characteristic of the three lowest quasi-degenerate states and since at 4 K only the lowest state can emit, they proposed that the emission occurs from a S_1 state of mixed T_{1g}, T_{2g} and G_g character. Differences in the relative vibronic band intensities between the Ne and Ar matrix spectra were attributed to differences in the relative contributions of the three quasi-degenerate lowest excited states to the emitting level in

the two matrices. This observation results from different matrix perturbations acting on the C_{60} solute molecule in Ne and Ar matrices. This analysis is pictorially shown in Fig. 3 where the

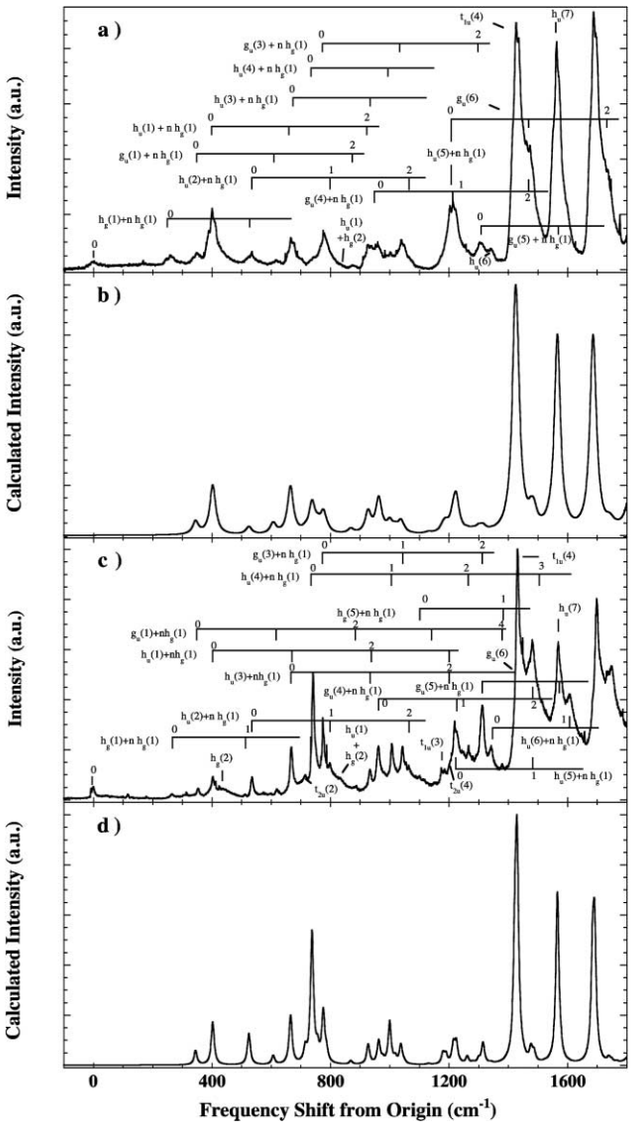

Fig. 3 (a) Fluorescence spectrum of C_{60} in a Ne matrix at 4 K in the 0–1800 cm^{-1} region. (b) Simulation of the fluorescence spectrum based on computed oscillator strengths (Table 4) and Franck–Condon activities. The contributions of the T_{1g}, T_{2g} and G_g states to the emitting level is assumed to be respectively 37, 56, and 7%. (c) As for (a), but for an Ar matrix. (d) The same as for (b), but the contributions of the T_{1g}, T_{2g} and G_g states to the emitting level is assumed to be respectively 50, 25, and 25% (from ref. 6).

emission spectra in Ne and Ar, and the simulated spectra obtained from the computed intensities for the T_{1g}, T_{2g} and G_g states are displayed.

From the simulated spectra the contributions of the T_{1g}, T_{2g} and G_g states to the emitting level were found to be, respectively, 37, 56 and 7% for neon and 50, 25 and 25% for argon matrices.[6,35] These results suggest that in the neon matrix the T_{1g} and T_{2g} states are quasi-degenerate while the G_g state is somewhat higher, although less than 100 cm^{-1}. The argon matrix appears to mix the three states more extensively than neon, in particular the percentage of G_g character in S_1 is larger than in neon. This agrees with the notion that argon matrix perturbations are stronger than neon matrix perturbations.

In Table 5 we collect the vibronic bands observed in the fluorescence spectra measured in a Ne matrix at 4 K by Sassara *et al.*,[6,35] in a Ne matrix at 5 K by Hung *et al.*,[34] in a DC matrix at 1.2 K by van den Heuvel *et al.*,[33] in toluene matrix at 5 K by Rice *et al.*[36] and in a crystal at 1.2 K by van den Heuvel *et al.*[37] Note that, for the fluorescence spectra recorded in a Ne matrix by Hung *et al.*,[34] we prefer to attribute to the 0–0 band the energy of 15633 cm^{-1} rather than the value of 15648 cm^{-1} as proposed by the authors. As it is clear from Table 5, our choice places the origin closer to the 0–0 band observed by Sassara *et al.*[6] and renders the vibrational intervals more similar to the usual values of vibrational frequencies.

The calculated vibronic intensities allow one to assign practically all the vibronic bands appearing in the fluorescence spectrum in terms of false origins and of combination bands and to indicate which of three electronic state components of S_1, namely T_{1g}, T_{2g} or G_g, is the main promoter of each vibronic band.

The assignment of vibronic bands proposed in Table 5 follows mostly the assignment of refs. 6, 29 and 36. It emerges clearly that the most intense false origins are associated with the T_{1g} and T_{2g} states and are found in the 1400–1600 cm^{-1} frequency range. The remarkable FC activity in combination bands of the 266 cm^{-1} h_g mode is notable among all the h_g and a_g modes. It is worth noting that a weak origin band is observed in all matrices. In the unperturbed C_{60} molecule, the origin of fluorescence should be missing. Its appearance indicates that matrix interactions can mix to some extent the T_{1g} or T_{2g} or G_g, states with T_{1u} states of C_{60}, separated by at least 1 eV, inducing an allowed component of fluorescence or, alternatively, that some fullerene–solvent intermolecular motion acts as an inducing mode.

The comparison of the high resolution fluorescence spectra obtained in different matrices and summarized in Table 5 shows a remarkable agreement among the vibrational frequencies implied in the vibrational structure. Obviously, the different matrices do influence the intensity distribution by changing the character of S_1, which results from the mixing of the three quasi-degenerate symmetry states, and by adding their specific interactions on the C_{60} molecule.

Fluorescence spectra in Ne and Ar matrices at 4 K have been extended by Sassara *et al.*[6] up to 3500 cm^{-1} from the origin. The region from 1600 to 3500 cm^{-1} shows many combination bands based on the false origins $t_{1u}(4)$, $g_u(6)$, $h_u(7)$, $h_u(5)$, $g_u(4)$, on which progressions based on n quanta of the $h_g(1)$ mode are built. It is possible to identify also the bands due to the series $t_{1u}(4) + a_g(2) + nh_g(1)$, $g_u(6) + a_g(2) + nh_g(1)$, $h_u(7) + a_g(2) + nh_g(1)$, $h_u(5) + a_g(2) + nh_g(1)$, and $g_u(4) + a_g(2) + nh_g(1)$. The bands appearing in this region underscore the activity of the higher frequency mode $a_g(2)$, at 1468 cm^{-1}, predicted by the calculations.[6]

The energies of the 0–0 bands in the fluorescence spectrum for various environments are the following: 15633 cm^{-1} in Ne at 5 K; 15627 cm^{-1} in Ne at 4 K; 15487 cm^{-1} in Ar at 4 K; 15200 cm^{-1} in DC at 1.2 K; 15012 cm^{-1} in toluene at 5 K; 14629 cm^{-1} in a single crystal at 1.2 K.

Since the matrix made of light noble gas atoms interacts very weakly with the C_{60} solute, the energy of 15630 cm^{-1}, relative to the Ne matrix, should approach the corresponding energy in the gas phase. If, following Chergui,[38] we estimate the gas-phase to Ne matrix red shift to be 35 cm^{-1} and assume the Stokes shift to be from 10 to 30 cm^{-1} for the different electronic states, we can expect that the 0–0 band of the excitation spectra in the Ne matrix is in the range 15638–15648 cm^{-1}. For the same reason, the lowest electronic origin in the gas phase is expected to be between 15673 and 15683 cm^{-1}.

The measured S_1 lifetime in different matrices ranges from 0.9 to 1.5 ns.[24,38–40] The S_1 deactivation proceeds *via* inter-system crossing (ISC) to T_1 with a quantum yield close to 1. The weak dependence of the S_1 lifetime on the environment suggests that the three quasi-degenerate states have a similar decay rate.

3.4.2 Absorption–excitation spectra. The low energy region of the absorption spectrum, from 640 to 515 nm, was invest-

Table 5 Analysis of the fluorescence spectrum of C_{60} in several matrices (frequencies in cm^{-1})

Ne matrix, 4 K [a] 0–0: 15627	Ne matrix, 5 K [b] 0–0: 15633	Decalin–cyclohexane, 1.2 K [c] 0–0: 15200	Toluene, 5 K [d] 0–0: 15627	Crystal, 1.2 K [e] 0–0: 15627	Assignment	Fundamental frequency and combination bands [f]	Dominant electronic state
262	257	261	263	259	$h_g(1)$	266	T_{2g}
352			352	343	$g_u(1)$	345	T_{2g}
402	397	396	401	394	$h_u(1)$	403	T_{2g}
437					$h_g(2)$	431	T_{2g}
536	527	522	534	527	$h_u(2)$	525	G_g
616					$g_u(1) + h_g(1)$	611	T_{2g}
668	664	671	667	661	$h_u(1) + h_g(1)$; $h_u(3)$	667; 669	G_g; T_{2g}
714			715		$t_{2u}(2)$	715	G_g
743		749	738	732	$h_u(4)$	738	G_g
			754	761	$g_u(2)$	757	G_g; T_{2g}
776			776		$g_u(3)$	776	G_g
797	785		794		$h_u(2) + h_g(1)$	791	G_g
832			834		$h_u(1) + h_g(2)$	834	T_{2g}
881					$g_u(1) + 2h_g(1)$	887	T_{2g}
936			937		$h_u(3) + h_g(1)$	933	G_g
961	956	963	961	956	$g_u(4)$	963	G_g; T_{2g}
1003		1006	1005	1000	$h_u(4) + h_g(1)$	1004	G_g
			1021		$g_u(2) + h_g(1)$	1023	G_g; T_{2g}
1042	1045		1042		$g_u(3) + h_g(1)$	1042	G_g
1063			1064		$h_u(2) + 2h_g(1)$	1057	G_g
1185			1180		$t_{1u}(3)$	1180	T_{1g}
1204			1199		$h_u(1) + 3h_g(1)$	1201	T_{2g}
1216	1219	1222	1216		$h_u(5)$; $g_u(4) + h_g(1)$	1215; 1222	T_{1g}; T_{2g}
1265					$h_u(4) + 2h_g(1)$	1270	G_g
			1288		$g_u(2) + 2h_g(1)$	1289	G_g
1310	1317		1310		$g_u(5)$;$g_u(3) + 2h_g(1)$	1315; 1308	G_g
1342			1344		$h_u(6)$	1342	G_g
1380							
1426			1413		$g_u(6)$	1410	T_{2g}
1433	1437	1445	1433		$t_{1u}(4)$	1430	T_{1g}
			1442		$t_{1u}(3) + h_g(1)$	1446	T_{1g}
			1463		$a_g(2)$;$t_{2u}(4) + h_g(1)$	1456; 1468	T_{1g}; T_{2g}
1477	1480		1488		$h_u(5) + h_g(1)$	1488	T_{1g}
1525					$h_u(4) + 3h_g(1)$	1536	G_g
			1549		$g_u(2) + 3h_g(1)$	1554	G_g; T_{2g}
1567	1572	1563	1569		$h_u(7)$	1566	T_{2g}
			1583		$g_u(5) + h_g(1)$	1581	G_g
1606			1604		$h_u(6) + h_g(1)$	1608	G_g
			1672		$g_u(6) + h_g(1)$	1676	T_{2g}
	1701		1697	1692	$t_{1u}(4) + h_g(1)$	1696	T_{2g}

[a] From ref. 6. [b] From ref. 34. The origin was given at 15648 cm^{-1}. Our choice is closer to the origin reported in ref. 6 and gives frequency shifts closer to vibrational frequencies. [c] From ref. 33. [d] From ref. 36. [e] From ref. 37. [f] From refs. 31 and 6.

igated extensively with the purpose of assigning the vibrational structure and of disentangling the three lowest electronic states. Notable attention was given also to the spectral region 410–360 nm encompassing the first T_{1u} absorption. We start by discussing the lowest energy spectral region.

Several absorption or excitation spectra of C_{60} in low temperature inert matrices, giving a well resolved vibrational structure, have been measured.

Smalley and co-workers [23] obtained the resonant two-photon ionization spectrum (TPI) in the 635–595 nm range of cold, isolated, C_{60} molecules in a supersonic beam. Recently, Hansen *et al.*[41] repeated the same experiment obtaining a very similar spectrum. The well detailed structure of this spectrum has, so far, been assigned only partially,[29,38] and the origin(s) of the electronic transition(s) have not been determined with confidence. We shall discuss this spectrum presently. Groenen and co-workers [33] measured the excitation spectrum of C_{60} in a DC matrix at 1.2 K. Subsequently, Hung *et al.*[34] and Sassara *et al.*[6] obtained fluorescence excitation spectra of C_{60} in Ne matrices providing a wealth of vibronic details. More recently, Close *et al.*[24] observed the C_{60}–He droplet beam depletion spectrum (an excitation spectrum equivalent to an absorption spectrum) showing a resolution and a wealth of details comparable to the spectrum taken in supersonic beams.[23]

In Fig. 4 we display the excitation spectrum observed in Ne matrices at 4 K [6] together with its simulation on the basis of computed HT and FC activities. In Table 6 we report the energies of over 30 vibronic bands observed in the 0–1640 cm^{-1} interval of this spectrum and in the Hung *et al.* excitation spectrum,[34] and we present their assignment.

The central problem for the assignment of these spectra is the correct identification of the origin(s) of the three lowest electronic states, which all contribute to this spectral region. From the analysis of the fluorescence and the fluorescence–excitation spectra of C_{60} in the DC matrix,[33] Negri *et al.*[29] proposed that, in this matrix, the G_g state was higher than the T_{1g} state by 110 cm^{-1}. Later, Groenen and co-workers determined this gap by temperature dependent studies to be roughly 100 cm^{-1}.[25]

In their analysis of C_{60} spectra in the Ne matrix, Sassara *et al.*[6] noted that using a common origin (at 15659 cm^{-1}) for all the vibronic bands in the excitation spectrum, the frequencies of vibrations associated with the G_g state were found to be higher by about 40 cm^{-1} than the corresponding vibrational frequencies of the ground state. At the same time, the vibrational frequencies associated with the T_{2g} and T_{1g} states were lower by about 20 cm^{-1}. Since there is no obvious reason for such systematic differences between the vibrational frequencies of similar (originating from the same electronic configuration) states, it was concluded [6] that the G_g state was higher than T_{1g} and T_{2g} by about 60 cm^{-1}. On this basis, the electronic origins of the T_{1g} and T_{2g} states can be assumed to be roughly

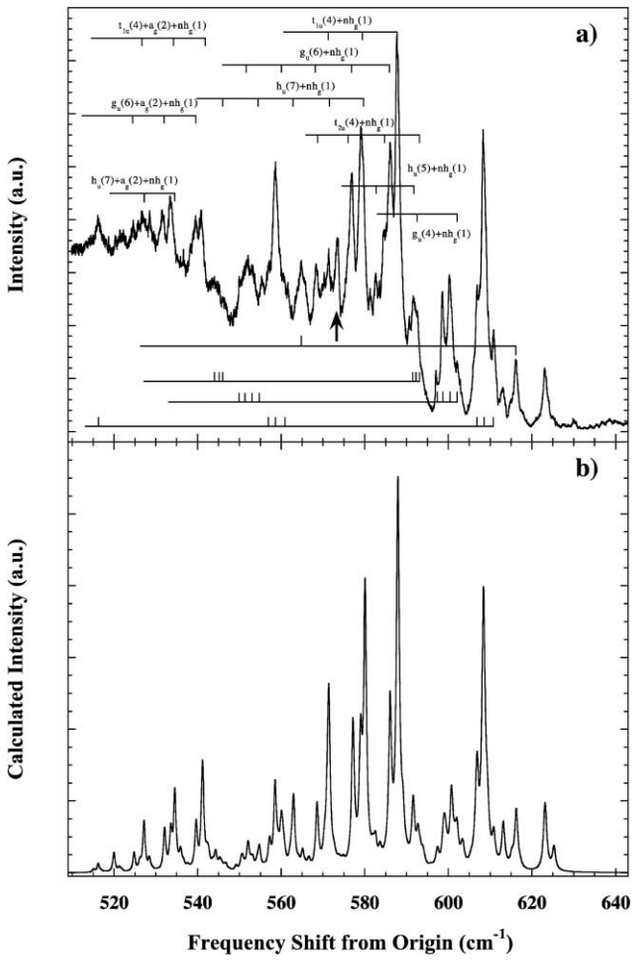

Fig. 4 (a) Fluorescence excitation spectrum of C_{60} in a Ne matrix at 4 K. The assignments for the short wavelength part are given and the remainder are discussed in the text. The band marked by an arrow corresponds to the $h_g(3)/g_g(3)$ modes of the state T_{2u}. (b) Simulation of the excitation spectrum based on computed oscillator strength and Franck–Condon activities (from ref. 6).

degenerate, within 10 cm^{-1}, and to be at the energy of 15644 cm^{-1}, a value compatible with the energy of the fluorescence origin (see above). The electronic origin of the G_g state is chosen to be 55 cm^{-1} higher, at the energy of 15699 cm^{-1}. In this way, the vibrational frequencies of the three excited states are similar, with the notable exception of the mode $t_{1u}(4)$. Note that the T_{1g}/T_{2g} electronic energy is only slightly above the origin of fluorescence (15627/15633 cm^{-1} see Table 6) implying a tiny Stokes shift.

It may be surprising that T_{1g} and T_{2g} states are quasi-degenerate, and that the $t_{1u}(4)$ frequency drops to 1370 cm^{-1} in the excitation spectrum, by about 60 cm^{-1} with respect to the ground state. However, this choice appears to be without obvious alternatives, since the lowest electronic origin has to be above the fluorescence origin. Recently, Chergui and co-workers,[26] by studies of the time-dependent fluorescence spectropy in a Ne matrix, found that the bands associated with the T_{1g} and T_{2g} character show a short component rise (*ca.* 170 ps) followed by a slower decay, with a decay constant of 900 ps. The time evolution of the vibronic bands associated with the G_g state are characterized by a bi-exponential decay, with two decay constants of 130 and 900 ps. These experiments indicate that the T_{1g} and T_{2g} states follow similar relaxation dynamics based on the ISC to the triplet manifold, while the G_g state appears to decay faster through an internal conversion (IC) channel leading to the two lower singlet states. Therefore, these observations appear to support the picture that in the Ne matrix the T_{1g} and T_{2g} states are roughly degenerate and well separated from G_g.

Recently, Sassara *et al.*[26] have proposed that the three lowest excited singlet states (S_1, S_2 and S_3) in the Ne matrix are equally separated in energy ($\Delta\nu$ about 50 cm^{-1}) with the lowest state S_1 (T_{1g}) lying at 15644 cm^{-1} followed by the T_{2g} and G_g levels, respectively at *ca.* 15694 and 15744 cm^{-1}. However, an explicit and detailed reassignment on the basis of the excitation spectra in the Ne matrix has not been given and only some of the bands in the supersonic beam spectrum of Smalley *et al.*[23] have been assigned.

We now discuss the assignments, presented in Table 6, of the excitation spectrum measured in a Ne matrix. For most of the bands, we follow the assignment proposed in ref. 6 but for some, alternative attributions are proposed. The intense band at 600.4 nm, 1011 cm^{-1} above the lowest electronic origin, was interpreted in ref. 6 as a combination band, $h_u(4)$ + 215 cm^{-1}. The latter frequency, not found in the ground state, was assumed to be associated with a mode of $h_g(1)$ parentage, resulting from the JT interaction occurring in the degenerate G_g state. It is at least as plausible to assign the 1011 cm^{-1} band as the combination $h_u(4) + h_g(1)$ based on the T_{2g} state, obtaining its intensity from the pseudo-JT coupling between T_{2g} and G_g states, induced by the $h_g(1)$ mode. It is attractive to consider a further alternative assignment, that the 1011 cm^{-1} band is the false origin associated with another electronic state, namely the $1H_g$ state, calculated to be 0.4 eV above the G_g state (see Table 3). If, specifically, the band at 1011 cm^{-1} is interpreted as the false origin due to the $t_{2u}(2)$ mode of 715 cm^{-1} (see Table 4), then the origin of the H_g state would be found 296 cm^{-1} above S_1. As we shall see below, this assignment is compatible also with the analysis of the supersonic beam C_{60} spectrum of Smalley and co-workers.[23]

Furthermore, we modify the assignments of the bands at 593.8 nm (16841 cm^{-1}), 593 nm (16863 cm^{-1}) and 580.1 nm (17238 cm^{-1}) which are now interpreted as the false origins $t_{1u}(3)$, $h_u(5)$ and the combination band $h_u(4) + 3h_g(1)$, respectively, associated with the T_{1g}/T_{2g} electronic states. Note that the band marked with an arrow in Fig. 4, observed at 573.4 nm, that is 1796 cm^{-1} above S_1, was attributed in ref. 6 to the false origins $g_g(3)$ and $h_g(3)$, with frequencies 738 and 709 cm^{-1}, respectively, associated with the state T_{2u}, which immediately follows the state H_g. The origin of this state would be about 1080cm^{-1} above S_1. With respect to the fluorecence spectrum, only one frequency shows a notable change, namely the frequency of the $t_{1u}(4)$ mode, associated to the state T_{1g}, which drops from 1430 to 1370 cm^{-1}. As discussed in ref. 6 one source of such decrease is the vibronic coupling between T_{1g} and the state $1H_u$ calculated to be above T_{1g} by 0.7 eV.

We consider now the classical C_{60} excitation spectrum in supersonic beams[23] and the recent spectrum in He droplets[24] in the spectral range 630–595 nm, which are very rich in vibrational structure. The He droplet is an ideal, very inert medium for a solute to be studied, since it causes a negligible red shift and is believed to induce no symmetry lowering. In fact, the He droplet spectrum of C_{60} is very similar in resolution and band energies to the supersonic beam spectrum, as can be seen in Table 7, where the energies of the observed bands are given. Fig. 5 displays the spectrum in supersonic beams[23] in which all the bands reported in Table 7 are numbered.

The determination of the electronic origin(s), unobserved in the unperturbed molecule, is fundamental for the assignment of these spectra. Since in the Ne matrix the lowest electronic origins in the fluorescence and in the excitation spectra are at 15630 and 15644 cm^{-1}, respectively, the S_1 origin in the isolated molecule is expected to be at 15673/15683 cm^{-1} (*vide supra*). The intense vibronic bands at 16228, 16436 and 16477 cm^{-1} are naturally assigned to the modes $h_u(2)$, $h_u(4)$ and $g_u(3)$, respectively, based on the G_g state. The energy of the electronic origin of this state is then fixed at 15740 cm^{-1}, in agreement with Chergui[38] and Negri *et al.*[29] The vibronic bands observed at 16035 and 16085 cm^{-1}, assigned to the modes $g_u(1)$ and $h_u(1)$,

Table 6 Vibronic assignment of excitation spectra of the C_{60} molecule isolated in a low temperature Ne matrix (energies in cm^{-1})

Neon matrix, 4 K [a]			Neon matrix, 5 K [b]		Assignment [c]			
Band energies	Shift from T_{1g}, T_{2g} 0–0: 15644	Shift from G_g 0–0: 15699	Shift from T_{1g}, T_{2g} 0–0: 15644	Shift from G_g 0–0: 15694	On T_{1g}, T_{2g} states	On G_g state	Vibronic frequencies	Shift from H_g state 0–0: 15940
15869	225		222		$h_g(1)$		266	
			282		$h_g(1)$		266	
15992	348				$g_u(1)$		345	
16046	402	347	399	349	$h_u(1)$	$g_u(1)$	403, 345	
16228		529		528		$h_u(2)$	525	
16257	613		605		$g_u(1) + h_g(1)$		611	
16311	667	612	663	613	$h_u(1) + h_g(1)$; $h_u(3)$	$g_u(1) + h_g(1)$	669, 697, 611	
16369		670		667		$h_u(3)$	667	
16409	765	710	780	730	$g_u(2)$, $g_u(3)$	$t_{2u}(2)$	757, 776, 715	
16436		737		737		$h_u(4)$	738	
16477		778		785		$g_u(3)$	776	
16499		800				$h_u(2) + h_g(1)$	791	
16515	871				$g_u(1) + 2h_g(1)$		877	
16576	932	871			$667 + h_g(1)$	$611 + h_g(1)$	933, 877	
16609	965		953		$g_u(4)$		963	
16631		932		934		$667 + h_g(1)$	933	
16655	1011	956	1005	955	$h_u(4) + h_g(1)$	$h_u(4) + 215$	953	715 $t_{2u}(2)$
16708		1009		1006		$h_u(4) + h_g(1)$	1004	
16742		1043		1045		$g_u(2) + h_g(1)$	1023	
16841	1197				$t_{1u}(3)$		1180	
16863	1219		1229		$h_u(5)$		1215	
16904		1205		1205		$t_{2u}(4)$	1190	
16932		1233		1225		$h_u(5)$	1215	
16969		1270				$h_u(4) + 2h_g(1)$	1270	
17016	1372	1317	1362	1307	$t_{1u}(4)$	$g_u(5)$	1430, 1315	
17062	1418		1409		$g_u(6)$		1410	
17100	1456				$t_{1u}(3) + h_g(1)$		1446	
17159		1460				$t_{2u}(4) + h_g(1)$	1456	
17197	1553				$h_u(7)$		1567	
17238		1539				$h_u(4) + 3h_g(1)$	1537	
17268	1634				$t_{1u}(4) + h_g(1)$		1638	

[a] From ref. 6. [b] From ref. 34. [c] From ref. 6 with some modifications, see text.

Table 7 Vibronic assignment of excitation spectra in a supersonic beam and in He-droplets of the C_{60} molecule (energies in cm^{-1})

Gas phase TPI spectrum [a]			He-droplet spectrum [b]		Assignment [c]			
Band energies	Shift from T_{1g}, T_{2g} 0–0: 15691	Shift from G_g 0–0: 15740	Shift from T_{1g}, T_{2g} 0–0: 15690	Shift from G_g 0–0: 15738	On T_{1g}, T_{2g} states	On G_g state	Vibronic. frequencies	Shift from H_g state 0–0: 15987
1–16035	344		345		$g_u(1)$		345	
2–16085	394	345	394	346	$h_u(1)$	$g_u(1)$	403, 345	
3–16207	516		533*		$h_u(2)$		525	
4–16263		523		525		$h_u(2)$	525	
5–16299	608		608*		$g_u(1) + h_g(1)$		611	
6–16333	642							345 $g_u(1)$
7–16353	662	613	654	606	$h_u(1) + h_g(1)$	$G_u(1) + h_g(1)$	667, 611	
8–16409		669		666		$h_u(3)$	667	
9–16434	743		742*		$h_u(4)$		738	
10–16444	753		757		$g_u(2)$		757	
11–16458		718		726		$t_{2u}(2)$	715	
12–16474	783	734	780	732	$g_u(3)$	$h_u(4)$	776, 738	
13–16496		756				$g_u(2)$	757	
14–16520		780		773		$g_u(3)$	776	
15–16538		798		796		$H_u(2) + h_g(1)$	791	
16–16563	872				$g_u(1) + 2h_g(1)$		877	
17–16616	925		920		$h_u(3) + h_g(1)$		933	
18–16643	952		946*					667 $h_u(3)$
19–16657	966		957		$g_u(4)$		963	
20–16677		937		935		$H_u(3) + h_g(1)$	933	
21–16702	1011		1002		$h_u(4) + h_g(1)$		1004	715 $t_{2u}(2)$
22–16734		994		982		$t_{2u}(2) + h_g(1)$	981	
23–16750		1010		1002		$H_u(4) + h_g(1)$	1004	

[a] From the spectrum of ref. 23. [b] From ref. 24; asterisks mark frequencies read on the spectrum. [c] From the calculated intensities and frequencies of ref. 6.

respectively, of the T_{2g} state, imply the energy of 15691 cm^{-1} for the electronic origin of this state. The contribution of the T_{1g} state to the vibrational structure of this frequency range comes from the $h_u(1)$ and $h_u(4)$ false origins, shifted from the electronic origin by 403 and 738 cm^{-1}, respectively. The $h_u(1)$ band can be associated with the 16085 or with the 16035 cm^{-1} band. The

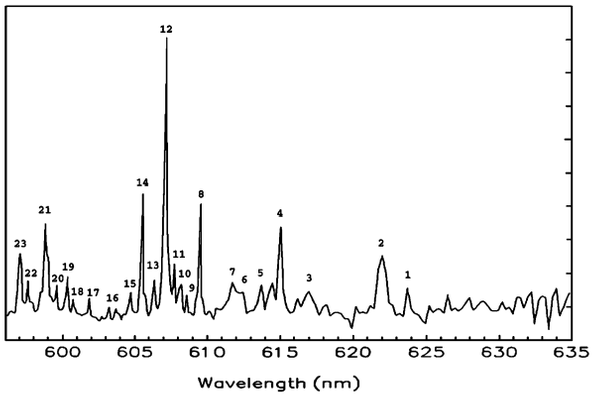

Fig. 5 Resonant two-photon ionization spectrum (from ref. 23) with bands assigned in Table 6 indicated.

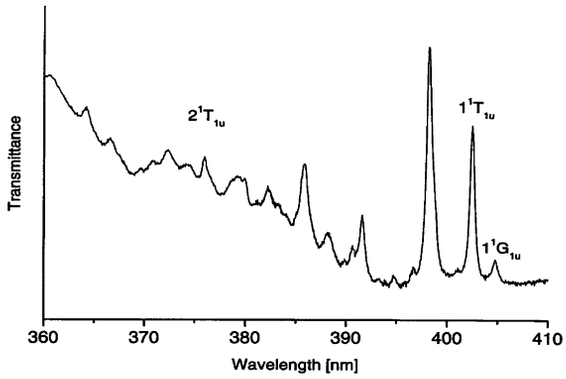

Fig. 6 Fluorescence excitation spectrum of C_{60} in a Ne matrix at 4 K in the 360–410 nm region with the assignment of three electronic states (from ref. 27).

electronic origin of the T_{1g} state would be in the latter case at 15632 $cm^{-1}$and in the former at 15690 cm^{-1}, the same energy of the T_{2g} state. Since it appears unlikely that the lowest electronic origin in the isolated molecule drops below the electronic origin in the absorption recorded in Ne matrix (15644 cm^{-1}), and that this matrix causes such a markedly different red shift for the T_{1g} and T_{2g} states, it is preferable to attribute roughly the same energy to the T_{1g} and T_{2g} electronic origins also in supersonic beams.

The spectrum of C_{60} in He droplets shows a wide band in the region of the forbidden electronic origins, implying a droplet induced intensity. This observation is surprising since He droplets are a most inert medium and, in fact, do not cause a red shift with respect to the spectrum in the supersonic beam.

In Table 7 we list 23, practically all, vibronic bands which correspond to the bands marked in Fig. 4. Most of them are assigned to false origins or combination bands associated with the G_g state. Some are associated with the T_{2g} state and only one exclusively with the T_{1g} state. Three bands, shifted by 642, 952 and 1011 cm^{-1} with respect to the lowest electronic origin, are tentatively assigned to false origins of the H_g state having its electronic origin at 15987 cm^{-1}. Hence, the supersonic beam spectrum also lends some support to the identification of vibronic bands of the H_g state in the low energy region of absorption–excitation spectra of C_{60}.

In conclusion, the available high resolution excitation spectra, assigned on the basis of the results of quantum chemical calculations, have allowed clarification in a consistent way of the ordering of the lowest three electronic states and their contributions to the rich vibronic structure observed in the Ne matrix, He-droplets and in supersonic beams. An extension of the spectral range of highly resolved spectra taken in supersonic beams, which could comprise all the vibrational structure of the lowest three electronic states, including the intense false origins of the T_{1g} state, would provide a precious test for the present analysis. In particular, it would allow testing of the still tentative proposal that the H_g and T_{2u} states are found within 1100 cm^{-1} of the state S_1. Finally, it is worth noting that the available spectra do not provide clear evidence of splittings of the degenerate vibrational modes due to Jahn–Teller effects or to matrix perturbations.

We consider now the 350–410 nm region of the C_{60} fluorescence–excitation spectrum which has been intensely investigated because it shows the contribution of the lowest *ungerade* states and specifically of the lowest T_{1u} state. Accordingly, this region has been studied in an Ar matrix,[28] in a methylcyclohexane–isopentane solid solution at 77 K,[23] in supersonic beams,[23] and recently in a Ne matrix.[27] This last spectrum is shown in Fig. 6.

This spectrum shows a large number of vibronic bands belonging to more than one electronic state. Two bands at 24839 and at 25113 cm^{-1}, separated by one $h_g(1)$ vibrational quantum, are very intense: these two bands have been assigned to the first allowed transition of C_{60}. The analysis of the entire vibronic structure observed in this region has led to the recognition of the contribution of two additional states, $1G_u$ and $2T_{1u}$. The analysis of the vibrational structure associated with these states has been discussed by Chergui and co-workers.[42]

3.5 Triplet state spectroscopy

C_{60} is a very promising candidate as a material for optical limiting devices[39,43] because of the sufficiently long lifetime of its lowest triplet state, T_1 (about 400 μs[44,45] in hydrocarbon matrices below 10 K), of the high efficiency ($\phi = 0.97$[40,46]) for the $S_1 \longrightarrow T_1$ ISC and thanks to the fairly high transient molar absorption coefficient in the visible spectral region.[43,46,47] In fact, C_{60} is almost transparent in the visible region under low optical intensities, when C_{60} molecules are virtually all in the ground state, but becomes increasingly absorbing when it is exposed to light of increasing intensity and a larger number of molecules are brought to the T_1 state.

According to calculations[5,15,16] the lowest triplet state is of g-type, as are the lowest singlet states, and specifically it belongs to the T_{2g} irreducible representation. The second triplet is found 0.4 eV above T_1,[48] a gap relatively large compared with the virtual degeneracy of the lowest excited singlets. Since the spin wavefunctions transform according T_{1g}, the phosphorescence process is symmetry and spin-multiplicity forbidden in C_{60} and it is induced by spin–orbit and vibronic interactions. As a consequence, this transition is extremely weak and can be enhanced by the external heavy-atom effect, which is obtained by dispersion of C_{60} in matrices containing heavy atoms. Furthermore, if the symmetry remains I_h, the 0–0 band will not be observed and, in analogy with the fluorescence spectrum, most of the vibrational structure will consist of false origins associated with HT inducing modes, together with a few combination bands. The latter involve totally-symmetric (TS) a_g modes and JT active h_g modes that, thanks to the displacement of the T_{2g} triplet equilibrium geometry with respect to the ground state structure, can form Franck–Condon progressions.

Several groups have studied the phosphorescence spectra of C_{60}.[45,49–51] The most recent spectra, taken in matrices at low temperature, by Sassara *et al.*[50] and by Groenen and others[45,51] show a sufficiently well resolved vibrational structure.

The first spectrum, displayed in Fig. 7, was measured in a Xe matrix at 30 K, and shows a highly resolved vibrational structure. It shows a strong 0–0 band, at 12714 cm^{-1}, followed by a progression of the $h_g(1)$ mode, on top of which one can recognize the weak bands due to u-type inducing modes. It does not provide information on the vibrational structure of the isolated molecule in the 0–700 cm^{-1} spectral range where the $h_g(1)$ progression accounts for most of the intensity. In the 700–2000 cm^{-1} frequency region, several bands are identified that

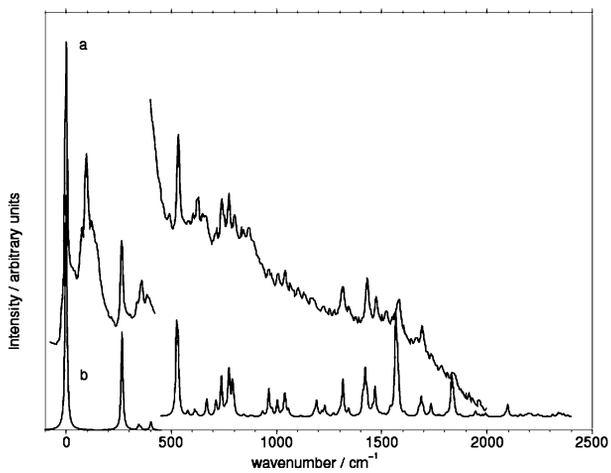

Fig. 7 Simulated and observed phosphorescence spectra of C_{60}. (a) The experimental spectrum obtained in the Xe matrix at 30 K (from ref. 50). (b) The simulated spectrum with a bandwidth of 5 cm^{-1}. A strong 0–0 band was added to the computed intensities for comparison with the observed spectrum (from ref. 48).

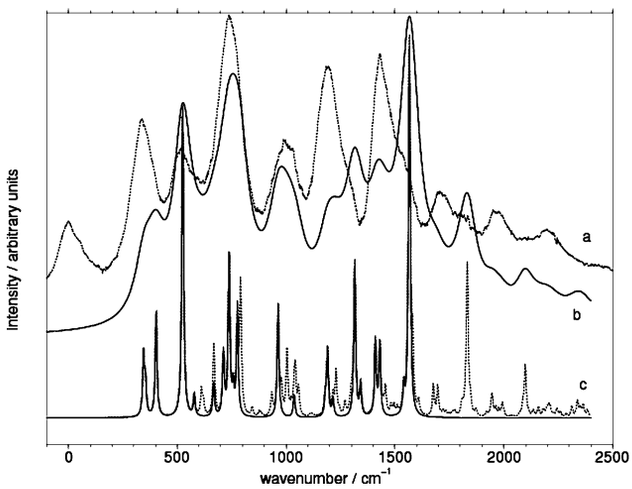

Fig. 8 Simulated and observed phosphorescence spectra of C_{60}. (a) The experimental spectrum obtained in the DC matrix at 1.5 K (from ref. 51). (b) The simulated spectrum with a bandwidth of 50 cm^{-1}. (c) The phosphorescence spectrum simulated with a bandwidth of 5 cm^{-1}. The solid line bands are HT induced false origins discussed in the text. The remaining bands are progressions and combinations of FC bands built on false origins.

can be due to the HT inducing modes, combination bands and to fundamentals of FC active modes. The observation of a strong 0–0 band indicates that one important side effect of Xe matrices is to lower effectively the symmetry of C_{60} and consequently to render the phosphorescence spectrum symmetry-allowed. As discussed by Sassara *et al.*[50] the observed spectrum is the superposition of the spectra of two sites, the second of which has a broader emission, approximately 100 cm^{-1} red-shifted, which can be easily distinguished from the former.

It is worth noting that a phosphorescence spectrum taken in an Ne matrix with 1.25 % of Xe[34] has qualitatively the same structure, albeit with lower resolution, as the spectrum measured in the Xe matrix, and shows a strong 0–0 band at 12773 cm^{-1}. Apparently, this small amount of Xe is sufficient to produce a significant heavy atom effect on the solute C_{60} molecules.

The phosphorescence spectrum measured in a DC matrix at 1.5 K, reported by van den Heuvel *et al.*,[45] was extended recently over a larger spectral range.[51] This spectrum is weaker and less resolved than the spectrum in the Xe matrix, presumably because it is emitted from a collection of molecules that experience many slightly different environments. However, it has the advantage that its 0–0 band is weak and thus all the observed vibronic bands can be assigned to HT active modes or to combination bands based on them. Thus, the two spectra are complementary and together they present a reasonable number of spectral features. The spectrum observed in the DC matrix, with the 0–0 band at 12530 cm^{-1}, is shown at the top of Fig. 8.

All the vibronic bands observed in the two spectra are collected in Table 8 and are assigned on the basis of calculated intensities of the false origins[48] and of the experimental vibrational frequencies of Schettino *et al.*[31] The calculations indicate that the largest vibronic activity is associated with the h_u modes with experimental frequencies of 403, 525, 738 and 1566 cm^{-1}, the g_u modes of 776, 963 and 1315 cm^{-1} and the t_{1u} mode of 525 cm^{-1}. The total oscillator strength of the unperturbed C_{60} phosphorescence, which is the sum of the oscillator strength of all the false origins, is very small (5.7×10^{-10}). This explains the very low quantum yield of the phosphorescence ($<10^{-4}$) and the difficulty encountered in detecting it without heavy-atom enhancement.

The calculations of the γ distortion parameters indicate that the FC mechanism is reasonably efficient only for the $h_g(1)$, $h_g(4)$, $h_g(7)$, $h_g(8)$ and $a_g(2)$ modes.[7]

In Figs. 7 and 8 the spectra simulated on the basis of calculated parameters are compared with the observed spectra. The simulation is performed by using two Lorentzian bandwidths of 50 and 5 cm^{-1}, respectively, to account for the different linewidth of the two experimental spectra. The comparison shows the following: (i) the agreement with the spectrum in the Xe matrix appears quite satisfactory; (ii) the agreement with the spectrum in the DC matrix is also satisfactory, but the bands of the simulated spectrum above 1200 cm^{-1} do not overlap exactly with the bands of this observed spectrum, while preserving the same intensity trend. A similar discrepancy also appears comparing the two experimental spectra.

The vibrational structure of the phosphorescence spectra of C_{60} in the DC matrix is dominated by false origins. A number of observed bands can be attributed to combination bands of inducing modes with FC active modes. Among the latter, important contributions to the vibrational structure are provided by the $h_g(1)$ mode and, to a lesser extent, to the $a_g(2)$ mode. The spectrum in the Xe matrix shows an intense true origin and thus the role of FC active modes is obviously more pronounced. In fact, progressions of TS and JT active modes, built on the 0–0 band, appear with strong intensity in the spectrum.

With respect to the assignment proposed by Sassara *et al.*,[46] based only on vibrational frequencies, some modifications are introduced in Table 8 concerning the bands at 771, 841, 1037 and 1468 cm^{-1}.

The properties of the state T_1 were also investigated by measuring the EEL spectrum of the triplet exciton of the (111) surface of solid C_{60} at 105 K.[7] The EEL spectroscopy, in which the molecule is excited by absorbing part of the kinetic energy of colliding electrons, is much less limited by symmetry and spin-multiplicity selection rules than conventional optical spectroscopy induced by interaction with the radiation's electromagnetic field.[52] By tuning the electron kinetic energy, one can also observe weak electronic transitions. In particular, near-threshold EEL spectra, in which the electron residual kinetic energy is close to zero, are dominated by singlet–triplet transitions which appear as allowed. The C_{60} S_0–T_1 EEL spectrum, measured in conditions of exchange scattering, shows a prominent 0–0 band and a vibrational structure based on Franck–Condon progressions of h_g and a_g modes.[7] The false origins, induced by the HT mechanism, are not observed in this spectrum because they are comparatively very weak. The vibrational structure is built mainly on the contributions of the modes $h_g(1)$, $h_g(4)$, $h_g(7)$, $h_g(8)$ and $a_g(2)$ which are also found to be active in phosphorescence (*vide supra*). Interestingly, the

Table 8 Analysis of phosphorescence spectra of C_{60} (frequencies in cm^{-1})

		HT active modes		FC active modes	
Xe, 30 K [a] 0–0: 12714	DC, 1.2 K [b] 0–0: 12530	Assignment [c]	Fundamental frequency and combination	Assignment	Fundamental frequency and combination
	345	$g_u(1)$, $h_u(1)$, $t_{2u}(1)$	345, 354, 403		
	520	$h_u(2)$, $t_{1u}(1)$	525, 525	$2h_g(1)$	532
710		$t_{2u}(2)$	715		
737	745	$h_u(4)$	738		
771		$g_u(3)$	776	$h_g(4)$	772
959		$g_u(4)$	963		
1007	995	$h_u(4) + h_g(1)$	1004		
1037	1030	$g_u(3) + h_g(1)$, $t_{2u}(3)$	1042, 1037		
1172	1190	$t_{1u}(3)$, $t_{2u}(4)$	1180, 1190		
1312		$g_u(3) + 2h_g(1)$, $g_u(5)$	1315, 1308		
1338		$h_u(6)$	1342		
1425	1435	$g_u(6)$, $t_{1u}(4)$	1410, 1430	$h_g(7)$	1421
1468		$t_{2u}(4) + h_g(1)$	1456	$a_g(2)$	1468
1573	1531	$g_u(5) + h_g(1)$, $h_u(7)$	1566, 1581	$h_g(8)$	1574
1686		$g_u(6) + h_g(1)$, $t_{1u}(4) + h_g(1)$	1696, 1676		
1734	1710	$t_{2u}(4) + 2\ h_g(1)$	1722	$a_g(2) + h_g(1)$	1734
1839	1840	$g_u(5) + 2h_g(1)$, $h_u(7) + h_g(1)$	1847, 1832	$h_g(8) + h_g(1)$	1840
1960	1935	$g_u(6) + 2\ h_g(1)$, $t_{1u}(4) + 2\ h_g(1)$	1942, 1962		
	2185	$h_u(4) + a_g(2)$	2206		

[a] From ref. 46. [b] From ref. 47. [c] From ref. 44.

same values of the γ parameters used to simulate the contribution of the a_g and h_g modes in the phosphorescence spectrum allow assignment and simulation of the vibrational structure of the EEL spectrum.[7] These results reveal that the perturbations due to the crystal field do not affect the structure of vibronic levels.

In conclusion, the vibrational structure of the phosphorescence and of the EEL spectra of C_{60} can be analyzed in a consistent way by making use of quantum-chemical simulations. Both analyses are based on the assignment of T_1 to the symmetry species T_{2g}. Since this state is well separated in energy from higher triplet states, its has a well defined character, at variance with the S_1 state, which results from the mixing of the T_{1g}, T_{2g} and G_g quasi-degenerate states. However, the C_{60} phosphorescence, because of its intrinsic weakness, is strongly influenced by the matrix perturbations.

4 C_{70}

In this section we summarize the most relevant results that have emerged from experimental and computational studies on the electronic structure and spectroscopy of the second most abundant fullerene, C_{70}. Although very similar in size to C_{60}, C_{70} shows rather different spectroscopic features, most of which can be rationalized in terms of its lower symmetry. In this sense, the effect of symmetry lowering manifested in C_{70} spectroscopy can be considered as a reference starting point for what can be expected for larger, and generally less symmetric, fullerenes and fullerene-derivatives.

Indeed, a fundamental difference, compared to C_{60}, appears clearly by considering the results of simple molecular orbital calculations: regardless of the energy order, the symmetries of the lowest two unoccupied MOs (e_1'' and a_1'') and highest two occupied MOs (e_1'' and a_2'') indicate that low energy one electron excitations in C_{70} give rise to dipole-allowed excited states of E_1' symmetry. Electronic transitions from the ground state to states belonging to the E_1' irreducible representation are dipole-allowed in D_{5h} symmetry. The presence of low lying allowed excited states in C_{70} is expected to add complexity to the electronic spectroscopy of this fullerene. Indeed, the absorption spectrum of C_{70} shows a much stronger intensity in the low energy region as compared to C_{60}.[19,53]

To unravel the order and the nature of the lowest excited states of C_{70}, both of singlet and triplet multiplicity, the availability of well resolved electronic spectra (absorption, fluorescence, phosphorescence) was of fundamental importance. However, nicely resolved spectra have become available only relatively recently. This, combined with the computational difficulties in predicting the exact order of the lowest excited states of C_{70} with a precision of few tens of cm^{-1}, resulted in a delay in the assignment of its lowest excited singlet states which was accomplished with satisfactory accuracy only recently.[25,54–56]

4.1 Singlet state spectroscopy

The identification of the nature of the lowest emitting singlet state of C_{70}, for the reasons outlined above, followed a difficult and controversial sequence of attributions. In the following we will start with a chronological description of fluorescence measurements, and compare the experimental data with the results of simulations in the end. We will close this section with a brief discussion of the high resolution absorption and excitation spectra measured in the visible region.

4.1.1 Fluorescence. In early studies[32,57] the fluorescence spectrum of C_{70} was measured at 77 K, in methylcyclohexane, and the origin of the fluorescence was assigned to the first band observed in the spectrum. With this assignment, the first vibronic band appeared at 164 cm^{-1} and most of the intensity was located at *ca.* 700–800 cm^{-1}. With the above assignment, the frequency of the first vibronic band was very far from the lowest predicted and observed vibrational frequencies of C_{70}[30] which fall around 200–220 cm^{-1}. Later studies[58,59] showed that the intensity of the band assigned as the origin in early studies, was indeed strongly dependent on temperature. A multiple state emission was suggested, and the origin of the lowest emission was reassigned to the second observed band (15207 cm^{-1}). With this assignment, most of the activity observed in fluorescence was concentrated at about 500–600 cm^{-1} from the origin. Such emission was assigned to the $1E_1' \longrightarrow 1A_1'$ transition and the vibronic structure was assigned to e_2' false origins.[59] In more recent studies[55,60] highly resolved fluorescence spectra were obtained in Shpol'skii matrices (*n*-pentane) at the temperature of liquid helium. These spectra provide a more precise assignment for the main vibronic peaks, although the structures of the spectra are complicated by the presence of multiplets due to emission from C_{70} molecules in different sites. The analysis carried out in ref. 55 of the multiplets observed for the origin

and the vibronic bands, provided strong evidence for the symmetry forbidden character of the $S_1 \longrightarrow S_0$ transition. The emitting state was assigned to A_2' symmetry and most vibronic peaks were assigned to infra-red active fundamentals of e_1' symmetry. The same authors[55] presented preliminary temperature dependent measurements in which emission from a higher excited state was observed. The temperature dependent emission was attributed to a dipole allowed $S_2 \longrightarrow S_0$ transition since most of the intensity was located on the origin band, consistent with the earlier observations of Argentine and co-workers.[58,59]

More recently, the fluorescence spectrum of C_{70} has been obtained in solid neon at 4 K.[56] The vibronic structure observed is very similar to the fluorescence spectra measured in *n*-pentane[55] and a weak origin is identified at 15524 cm^{-1}. This origin is assigned to the $A_2' \longrightarrow A_1'$ forbidden transition.[56] A second, prominent origin is observed at 15691 cm^{-1}, and assigned to the $E_1' \longrightarrow A_1'$ transition.[56] To support the assignment of the forbidden transition, a second emission spectrum was reported by the authors, obtained by direct excitation into the 15524 cm^{-1} band. As expected, in this second emission spectrum the $E_1' \longrightarrow A_1'$ transition and its associated vibronic structure disappears.[56] Thus, C_{70} reveals a very unusual spectroscopic characteristic: emission from S_1 and from an excited state above S_1. There are few molecules for which such behaviour has been observed, among which is the very well known azulene.[61] In the case of C_{70} the energy separation between the two emitting states is very small: 167 cm^{-1} in solid neon. This energy spacing is smaller than the smallest vibrational frequency of C_{70} in the lowest excited state, thus electronic energy cannot be converted intramolecularly into vibrational energy. Furthermore, electronic to vibrational energy conversion is also very inefficient through coupling with low frequency phonons of the neon matrix.[26]

More recent measurements[25] of the C_{70} fluorescence spectra in decalin–cyclohexane as a function of the temperature, and of the excitation spectra of C_{70} in *n*-pentane matrices have confirmed the presence of a second emitting singlet state, whose separation from S_1 is site dependent in an *n*-pentane matrix and ranges between 160 and 220 cm^{-1}. In decalin–cyclohexane the energy difference was reported to be 130 cm^{-1}. The intensity of the origin of the second emission was found to be temperature dependent, and increased with temperature as an effect of the thermally induced population redistribution between S_1 and the higher E_1' state. Fluorescence from the E_1' state was observed at 1.5 K, which, similarly to the conclusions drawn in ref. 56 indicated that radiationless deactivation of E_1' is a bottleneck and radiative decay can compete with it.

4.1.2 Singlet electronic states of C_{70} and modeling of vibronic intensities. With such a complex vibronic structure, it is obvious that the quantum-chemically predicted energy order of excited states is not sufficient, and conversely, modeling of vibronic intensities is fundamental.

Excited states of C_{70} were computed[18,62] both with semiempirical and with time-dependent density functional theory, but since in the following we will concentrate on the modeling of vibronic intensities associated with them, we will discuss the calculations of excited states at semiempirical level reported in ref. 54.

To obtain more reliable indications of the symmetry and nature of the lowest excited states of C_{70}, CI calculations were carried out using the CNDO/S hamiltonian and the Mataga parametrization.[4] The structure of C_{70} employed in these calculations was obtained with the QCFF/PI hamiltonian[3] as described in ref. 63. Initially the CI method selected included only single excitations (CIS), and several orbital spaces for the CI calculations were investigated. All these calculations suggested that the lowest excited state of C_{70} belongs to A_2' symmetry and is relatively well separated in energy from the second lowest excited state, in agreement with earlier excited state calcualtions carried out with the INDO/S + CIS semiempirical method.[62] In summary, at the CIS level of theory, the lowest singlet state of C_{70} is predicted to be a dipole-forbidden state, as in C_{60}. At variance with C_{60}, however, the lowest dipole-allowed excited states of C_{70} are predicted to be much closer to S_1, though not as close as the experimental evidence indicates.[55,56] The satisfactory description of electronic states and transition dipole moments is evident from the simulation of the absorption spectrum depicted in Fig. 9. The latter was

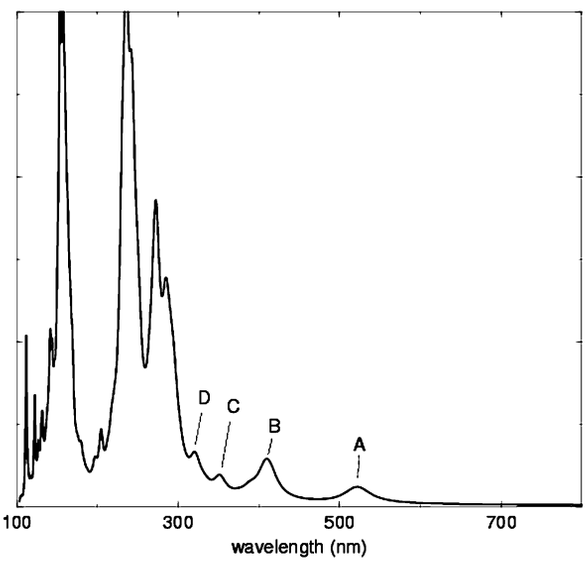

Fig. 9 The predicted electronic absorption spectrum of C_{70} from CNDO/S + CIS calculations (41 × 40 orbital space).

simulated on the basis of 41 × 40 CIS calculations, but similar results are obtained with smaller or larger CIS sizes.[64] The simulated spectrum shows two groups of strong bands, located at about 150 and 250 nm, respectively. These two strong clusters of bands are assigned to the strong absorption bands observed at 214 and 236 nm, respectively.[53] Interestingly, beside the two strongest bands observed at high energy, the simulated absorption spectrum of C_{70} reproduces closely the observed spectrum also in the lower energy region. The first four bands observed in hexane at *ca.* 468, 377, 359 and 330 nm[53] are easily identified with the first four prominent bands, labeled A, B, C and D in the simulation in Fig. 9. The latter are computed at *ca.* 523, 413, 352 and 320 nm, respectively. A more careful comparison between observed and simulated spectra shows that the energy of band A is underestimated by the calculations, a result unexpected since the method is known to overestimate singlet excitation energies.[5,6] Indeed, the excitation energies for the remaining three bands (B, C and D) are overestimated, as is the energy of the highest energy absorption in the spectrum (150 nm computed, *versus* 214 nm observed).

To improve the description of the lowest excited states of C_{70} CI calculations were carried out with the inclusion of double excitations, beside single excitations (CISD). The inclusion of doubly excited configurations dramatically affects the order of the lowest excited states of C_{70}, as can be seen from a comparison of CIS and CISD results collected in Table 9. The lowest excited state of C_{70} is still predicted to belong to A_2' symmetry, but four additional states are computed within 0.14 eV. The energy decrease of the $2A_2'$ and $2A_1'$ states is particularly remarkable. Furthermore, the lowest two E_1' excited states are inverted compared to CIS results. The weakest of the two is predicted to be the lowest, almost degenerate with the $1A_2'$, $2A_2'$ and $2A_1'$ states. Interestingly, the prediction of the lowest energy portion of the absorption spectrum improves considerably: band B is assigned to an A_2'' state, (see Table 9) in agreement with polarization measurements,[65] and the energy of band A increases.

Table 9 Effect of inclusion of doubly excitated configurations on excitation energies (E) and state ordering of the lowest singlet excited states of C_{70}

	CNDO/S + CIS (14 × 14)[a]			CNDO/S +CISD (14 × 14)[c]		
State	Symmetry	E/eV	Assignment[b]	Symmetry	E/eV	Assignment[b]
S_0	$1A_1'$	0.00		$1A_1'$	0.00	
S_1	$1A_2'$	2.13		$1A_2'$	2.44	
S_2	$1E_2'$	2.43		$2A_1'$	2.47	
S_3	$1E_1'$	2.47 (0.23)[d]	B and A	$1E_1'$	2.48 (0.002)	
S_4	$1A_2''$	2.48 (0.001)		$2A_2'$	2.58	
S_5	$2A_1'$	2.49		$1E_2'$	2.58	
S_6	$1E_1''$	2.57		$1E_1''$	2.71	
S_7	$2E_1'$	2.65 (0.004)		$2E_1'$	2.74 (0.13)	B and A
S_8	$2E_1''$	2.69		$1A_2''$	2.75 (0.001)	
S_9	$2A_2'$	2.70		$2E_1''$	2.97	
	$2A_2''$	3.11 (0.22)	B and B	$2A_2''$	3.27 (0.064)	B and B
	$3E_1'$	3.17 (0.42)	B and B	$3E_1'$	3.27 (0.005)	

[a] 196 singly excited configurations included. [b] Bands are labelled according to Fig. 9, see the text for discussion. [c] 1800 energy selected singly and doubly excited configurations. [d] Oscillator strength.

The above discussion on the prediction of electronic excited states of C_{70} makes evident, in analogy with C_{60}, an important intrinsic limit of molecular quantum chemical calculations, which is difficult to overcome: when several electronic states are predicted to be quasi-degenerate, as is the case for C_{60} and C_{70}, their energy order can be affected by changing the parameters employed in the calculations (geometrical structure, CI dimension, *etc.*). In this case the identification of the 'true' lowest excited state is critical and must be based on the simulation of its properties, among which, of crucial importance are the spectroscopic characteristics.

Thus, for C_{70}, the relevant result of CISD calculations shows that in the region of S_1 there is a congestion of electronic states, composed of several dipole-forbidden states and a dipole-allowed E_1' state. In order to assign the 'true' lowest singlet state, the vibronic activity was simulated for each of the low-lying excited states of C_{70} and compared with the observed spectra. In particular, three states were considered as possible candidates for S_1, beside the $1A_2'$state, namely the $2A_2'$ and $2A_1'$ states whose excitation energy is considerably lowered by inclusion of double excitations. Conversely, the predicted $1E_1'$ state was considered to be the only state responsible for the $S_2 \longrightarrow S_0$ emission. The small energy difference among these states and the presence of a dipole-allowed excited state separated from them by a few hundred cm^{-1}, makes impossible the use of the weak-coupling approach employed to investigate C_{60} singlet spectroscopy. A suitable model, in this case, must take into account electronic along with vibrational contributions to the energy gaps which separate vibronically coupled states. Thus, a perturbative approach that makes use of vibronic wavefunctions was adopted in this case to model the fluorescence spectrum of C_{70}. This approach was employed successfully to simulate the vibronic structure in the electronic and ZEKE spectra of naphthalene[66,67] and details on the method can be found in refs. 66 and 67.

Emission from the dipole-forbidden states of C_{70} occurs through the HT mechanism of intensity borrowing while emission from the E_1' state can be due to a combination of HT along with FC mechanisms. Thus the two possible mechanisms, depicted in Fig. 10 have to be considered. In the figure, for simplicity, we label with S_1 each of the three possible candidates for the lowest emitting state of C_{70}.

The required vibronic interactions were computed with the CNDO/S+CISD method. The simulated fluorescence spectra of the $1A_2'$, $2A_1'$ and $2A_2'$ states of C_{70} are presented in Fig. 11–13 where they are compared with the fluorescence spectrum observed in solid neon at 4 K.[56] All the spectra show a rich vibronic structure due to e_1' modes, but the intensity distribution is quite different for the three states. The simulation of the emission spectrum due to the $2A_2'$ state is particularly interesting, since most of the activity is predicted in the observed frequency region. Indeed, the strongest bands in the simulated spectrum, centered at 344, 388, 545, 766, 1114, and 1243 cm^{-1}, are readily assigned to the bands observed at 358, 412, 579, 793, 1082 and 1250 cm^{-1}.[56] It is interesting to note that this state is not predicted to be the lowest, but its energy is strongly affected by the inclusion of double excitations.

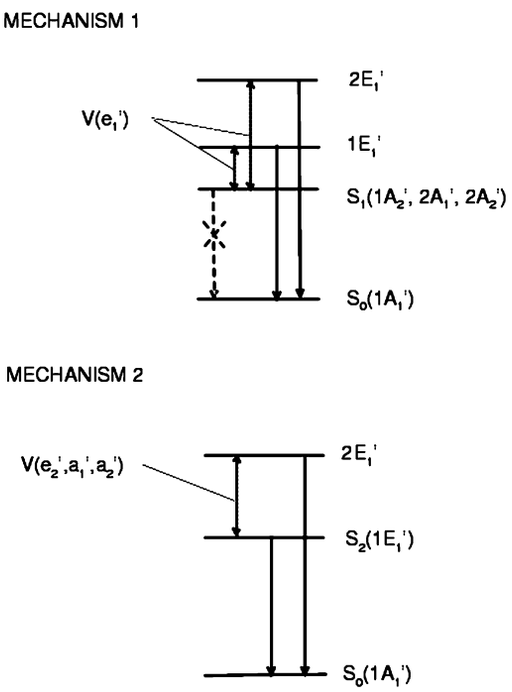

Fig. 10 Mechanisms of intensity borrowing for the $S_0 \leftrightarrow S_n$ transition of C_{70}. Electronic levels are indicated by horizontal solid lines; allowed (forbidden) transitions are represented by vertical solid (dashed) lines; vibronic interactions V(sym) mediated by vibrations of '*sym*' symmetry, are represented by dotted vertical lines. Mechanism 1 for emission from the $1A_2'$, $2A_2'$ and $2A_1'$ states. Intensity is stolen from $S_0 \longrightarrow E_1'$ transitions. Mechanism 2 for emission from the $1E_1'$ state.

In summary, the simulations show that the emission from the $2A_2'$ state accounts for most of the observed $S_1 \longrightarrow S_0$ vibronic activity. The emission predicted for the remaining two dipole-forbidden states agrees with the observed emission only in selected frequency regions. Nevertheless, the role of the $2A_1'$ state is more intriguing, since it is predicted to be very close to the $2A_2'$ state and its simulated emission shows some vibronic features very similar to the emission of the $2A_2'$ state and, consequently, very close to the observed vibronic structure. This is especially true in the lowest frequency region. For instance,

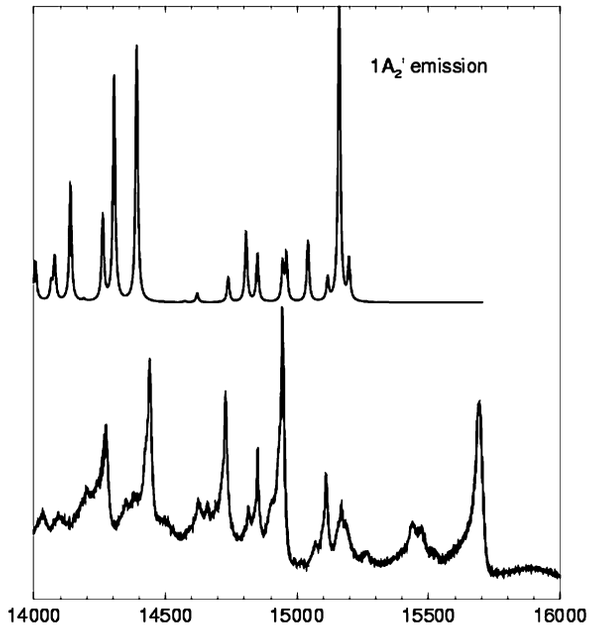

Fig. 11 (Top) computed $1A_2' \longrightarrow S_0$ emission and (bottom) fluorescence spectrum of C_{70} observed in solid neon.[56]

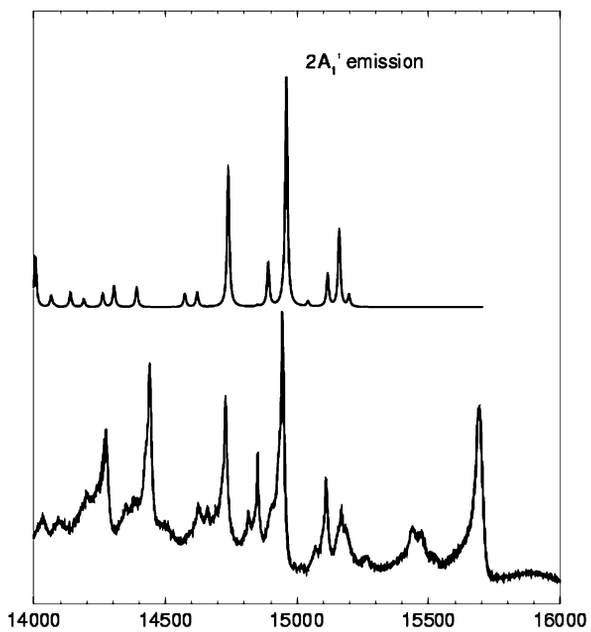

Fig. 12 (Top) computed $2A_1' \longrightarrow S_0$ emission and (bottom) fluorescence spectrum of C_{70} observed in solid neon.[56]

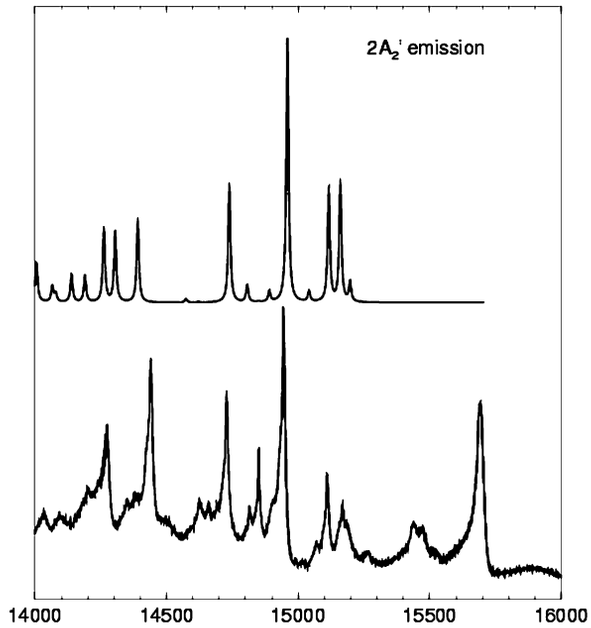

Fig. 13 (top) computed $2A_2' \longrightarrow S_0$ emission and (bottom) fluorescence spectrum of C_{70} observed in solid neon.[56]

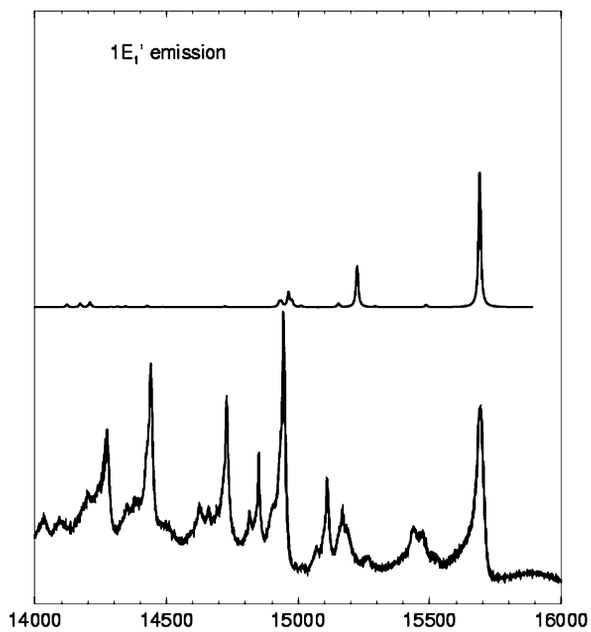

Fig. 14 Computed $1E_1' \longrightarrow S_0$ emission (top) and observed (bottom) fluorescence spectrum of C_{70} in solid neon.[56]

notice that most of the activity is computed at 344, 388, 545, 614 and 766 cm^{-1}, and these bands can be readily assigned to the bands observed at 358, 412, 579, 671 and 793 cm^{-1}. Conversely, the intensity is underestimated in the highest frequency region, above 1000 cm^{-1}. Minor perturbations, due to intra- or inter-molecular interactions might lower the symmetry of C_{70}, for instance to C_{5h}, and the two quasi-degenerate states, $2A_2'$ and $2A_1'$ might mix, without removing their dipole-forbidden character.

Concerning the second emitting state of C_{70}, the vibronically induced intensity of the $1E_1' \longrightarrow S_0$ transition can be borrowed from higher E_1' states *via* the e_2', a_1' and a_2' vibrations. In Fig. 14 the simulated spectrum is presented. It is seen that the vibronically induced intensity is very weak, except for the e_2' mode computed at 466 cm^{-1} with QCFF/PI calculations[30]). In addition, the FC and JT activity is predicted to be very weak[54] except for the lowest a_1' and e_2' frequencies. In summary, the simulations indicate that the $1E_1' \longrightarrow S_0$ transition should be dominated by its origin, in agreement with the observations from temperature dependent measurements[25,55,59] and in solid neon.[56]

4.1.3 Absorption–excitation spectra. Beside low resolution absorption spectra, more resolved spectra were obtained at low temperature.[23,25,56,68] The first measurement reported was the resonance two photon ionization (R2PI) spectrum, in a supersonic molecular beam, by Haufler *et al.*[23] This spectrum shows a dense structure of bands, some of which are clearly comparable to those observed in neon matrix, at 5 K, by Fulara *et al.*[68] The main difference between the two spectra is the presence of a rather strong 0–0 band in the spectrum of ref. 68 which is not seen in the R2PI spectrum since it is expected to appear at wavelengths greater than 635 nm, a region outside the range reported in ref. 23. The strong origin in the neon spectrum was assigned, correctly, to the $S_0 \longrightarrow 1E_1'$ transition, and the vibronic structure was attributed to e_2' JT active fundamentals. Recently,

Sassara *et al.*[56] reported highly structured fluorescence–excitation spectra of C_{70} in solid neon and proposed an assignment of all vibronic bands based on ground state vibrational frequencies of C_{70} obtained from vibrational spectroscopy and quantum-chemical calculations. The excitation spectrum (see Fig. 15) was interpreted as a superposition of three electronic

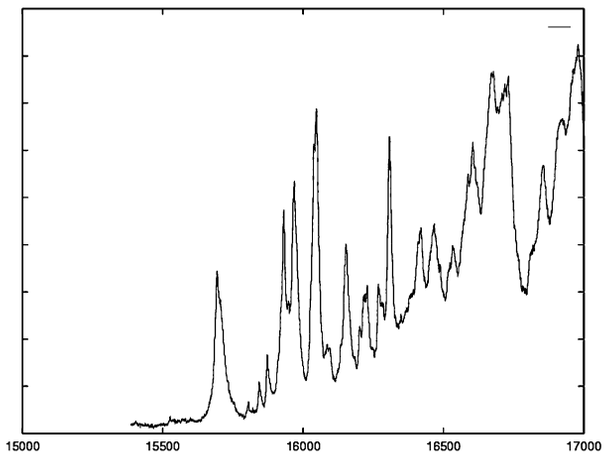

Fig. 15 Fluorescence–excitation spectrum of C_{70} in solid neon, from ref. 56. Energy in cm^{-1}.

transitions: $S_0 \longrightarrow A_2'$, $S_0 \longrightarrow E_1'$ and $S_0 \longrightarrow A_2''$. More recenty, Groenen and co-workers obtained highly resolved phosphorescence–excitation spectra of C_{70} in *n*-pentane at 1.5 K.[25] The vibronic structure observed in alkane matrices is very similar to the structure observed in neon matrix in refs. 68 or 56. The vibronic structure was assigned in term of the superposition of two electronic transitions: $S_0 \longrightarrow A_2'$, $S_0 \longrightarrow E_1'$.

To assign the complex vibronic structure in terms of simulated vibronic intensities, the perturbative approach based on vibronic basis sets, used to simulate the fluorescence spectra cannot be adopted. The only accurate approach must go beyond the Born–Oppenheimer (BO) approximation because of the closeness of interacting vibronic states.[69] Such modeling is however much more demanding, since several modes are vibronically acitive at the same time and several states are involved, and satisfactory results have not yet been obtained.

Nevertheless, a tentative assignment of the absorption spectrum can be made on the basis of simulated fluorescence intensities.

As discussed above, the simulations of fluorescence spectra confirm that the $S_0 \longrightarrow A_2'$ transition must be associated with a considerable vibronic structure, while the $S_0 \longrightarrow E_1'$ transition will be dominated by the origin. Thus, the bands observed in excitation[56] at 404 and 442 cm^{-1} are most probably related to the 412 cm^{-1} e_1' mode observed in fluorescence. Similarly the 518 cm^{-1} band observed in excitation is related to the 579 cm^{-1} band (e_1') observed as the strongest band in emission. The splitting of some of the stronger bands may be indicative of the contribution from more than one dipole-forbidden state (calculations predict at least three forbidden states). In addition, the apparent large frequency increase or decrease must be taken with caution, since it may merely reflect the effect of vibronic coupling which can depress (and mix) vibronic levels when these are below the interacting state (for instance the $2E_1'$ state) or push up vibronic levels when the interacting state is below (such as the $1E_1'$ state) the unperturbed vibronic level.

4.2 Triplet state spectroscopy

Similarly to the lowest triplet state of C_{60}, the triplet state of C_{70} has attracted a special interest in view of the optical limiting properties[2] that might derive from its efficient population combined with a triplet absorption cross-section which is higher than that of the ground singlet state in selected wavelength regions. The absorption spectrum of the triplet state of C_{70} shows indeed[70] a considerable cross-section at very low excitation energies (900–1100 nm). This characteristic might be used for some special applications of optical limiters in the near infrared region.

The lifetime of the lowest triplet of C_{70} was reported to be 53 ms, in toluene, by Wasielewski[44] and more recent measurements pointed to an averaged lifetime of the triplet substates of 51 ms in decalin–cyclohexane and in toluene.[71] Electron-spin-echo experiments enabled a complete description of the population and decay of the triplet substates at 1.2 K, and indicated that the decay to the ground state is about three times faster for molecules in the T_z sublevel than for molecules in T_x or T_y: *ca.* 90 ms *versus* 30 ms.[71] It is worth noting that such a lifetime is about 100 times longer than that of the lowest triplet of C_{60}.

Contrary to the lowest singlet state, the identification of the nature of the lowest triplet state of C_{70} was less controversial. Quantum-chemical CI calculations carried out with the CNDO/S hamiltonian indicated that the lowest triplet state of C_{70} belongs to the A_2' symmetry.[72] According to calculations T_1 is at least 0.2 eV from the next triplet state, but, more importantly, the simulation of the phosphorescence spectrum based on the $1A_2'$ triplet state is in good agreement with the observed spectrum.

For C_{70} the phosphorescence spectrum is easily observed, in contrast with the phosphorescence of C_{60}, and was measured at 77 K in saturated hydrocarbons[58,59] and more recently in toluene[60] and in *n*-pentane[55] at low temperature. The latter spectra show a well resolved structure that allowed a vibronic analysis of the spectrum. The onset of phosphorescence was measured at 12495 cm^{-1} in *n*-pentane and the most intense band in the spectrum appeared at 361 cm^{-1}.[55] Finally, the phosphorescence spectrum of C_{70} was recorded with very high resolution in solid neon at 5 K by Chergui and co-workers.[56] The main vibronic bands were assigned to e_1' modes and the lowest triplet state was assigned to the A_2' symmetry, in agreement with the results of quantum-chemical calculations.[72]

In Fig. 16 we compare the phosphorescence spectrum observed in solid neon[56] with the results of intensity modeling

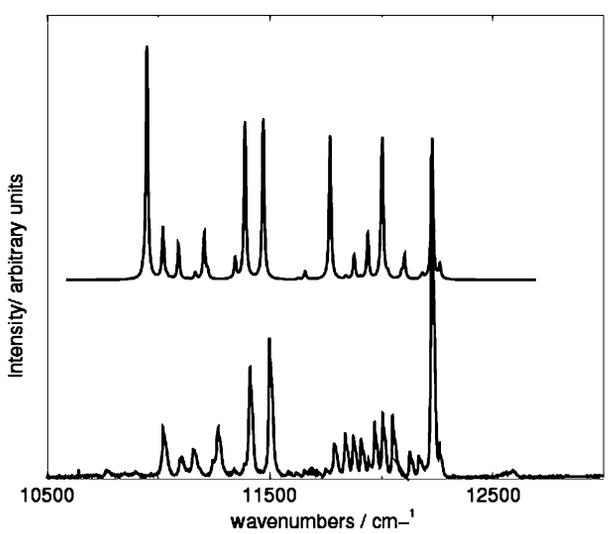

Fig. 16 (Top) computed and (bottom) observed phosphorescence spectrum of C_{70} in solid neon.[56]

based on quantum-chemical calculations. With T_1 belonging to A_2' symmetry, the $T_1 \longrightarrow S_0$ transition is symmetry as well spin-multiplicity forbidden. Indeed, in D_{5h} symmetry, triplet spin wavefunctions transform as A_2' and E_1'' irreducible representations, and dipole-moment Cartesian components along *x*, *y*, *z* transform as A_2'' and E_1' irreducible represent-

ations. Thus the transition is induced by SO coupling combined with vibronic perturbations mediated by modes that belong to the a_1'', a_2'', e_1' and e_2'' symmetry representations. Each of the modes belonging to these symmetry species may give rise to a false origin and thus contribute to the vibrational structure of the phosphorescence spectrum. In C_{70} there are nine a_1'', ten a_2'', twentyone e_1' and twenty e_2'' vibrations which need to be considered as possible promoters of false origins. In general TS vibrations too can contribute to the vibrational structure of electronic transitions through the FC mechanism. In fullerenes this mechanism, which is based on a displacement of the equilibrium geometry of the excited state with respect to the ground state, is rather inefficient. The FC activity was estimated in ref. 72 by computing the S_0 and T_1 equilibrium structures with the QCFF/PI hamiltonian[3] on the basis of ground state MOs. The resulting γ parameters are 0.09, 0.06, 0.05 and 0.34 for the a_1' modes whose computed frequencies are 1633, 1220, 1187 and 251 cm^{-1}, respectively. Thus, only the 251 cm^{-1} vibration might contribute to form combination bands in the observed spectrum.

The simulations presented in Fig. 16 were obtained by performing larger CI calculations compared to those published in ref. 72, namely an orbital space of 29 occupied and 29 virtual MOs was employed.

A summary of the experimental data, computed vibrational frequencies[30] and computed vibronically induced intensities is reported in Table 10. Experimental data are also compared with the vibrational frequencies of C_{70} recently computed with density functional theory (DFT) and the B3LYP functional.[73] The latter frequencies are very close to the fundamentals observed in vibrational spectroscopy studies, and offer a reliable guide for the assignment of the bands observed in phosphorescence. The agreement between observed and simulated spectra presented in Fig. 16 is very satisfactory, and most of the activity is due to e1′ modes. A closer inspection of simulated intensities shows some discrepancies in the intensity distribution: for instance, the observed intensity is distributed over several bands in the 550 cm^{-1} and 800 cm^{-1} regions, while it is concentrated on fewer bands in the simulations. In addition, the intensity is overestimated in the high frequency region, whilst it is underestimated in the low frequency region. Nevertheless, the agreement must be considered remarkable, since computed vibronic intensities result from the combinations of two perturbations: vibronic and spin–orbit, and are obtained by summing over a large nuber of small terms. The assignment proposed in Table 10 is based on computed vibronic intensities and makes use of the numerical values of DFT computed frequencies.[73] The main changes, compared to previous assignments,[56] concern the assignment of the observed 459 cm^{-1} band to a_2'' symmetry and the assignment of the 748 cm^{-1} band to e_2'' symmetry.

The accuracy of computed vibronic intensities can be checked by evaluating the average radiative rate constant for the three triplet sublevels, from the cumulative oscillator strength of all false origins. By employing the computed oscillator strengths, a lifetime of 0.11 s^{-1} was obtained in ref. 72. By considering the phopshorescence quantum yield of 1.3×10^{-3} and the triplet lifetime of 53 ms, measured in ref. 44 a radiative lifetime of 0.025 s^{-1} is obtained, which is of the same order of magnitude as the calculated value. The agreement provides support for the accuracy of the modeling and to the assignment of the phosphorescence spectrum.

5 Conclusions

In this paper we have reviewed some of the most important spectroscopic work aimed at clarifying the properties of the lowest excited states of C_{60} and C_{70}. We have stressed the role played by quantum chemical calculations in performing a sound analysis of the high quality spectra that are and will become available. In this context we have dwelled on the work in which we have been involved as well as on the spectroscopic results of the groups with which we have been in contact.

We have tried to show that we have reached a firm assignment of the ordering of the lowest excited states and of their interactions along with a detailed understanding of the vibronic structure of the phosphorescence, fluorescence and low energy absorption–excitation spectra of these large molecules. This analysis is based on some approximations, namely, the use of ground state vibrational frequencies, of the HT perturbation expansion and of the strong-coupling approach to account for the contributions of the h_g modes to combination band intensities and energies.

In the case of C_{60}, the three lowest excited singlet states, of *gerade* symmetry species, namely T_{1g}, T_{2g} and G_g, are quasi-degerate within 100 cm^{-1}. Thus, they mix under the perturbation of any matrix environment and this is reflected in vibrational structure changes of the fluorescence measured in different matrices. The high resolution excitation spectra, through an educated analysis guided by theory and computational results, reveal the size of the energy gaps existing between the lowest excited states. It is found that in supersonic beams, in He-droplets and in a Ne matrix, the states T_{1g} and T_{2g} are essentially degenerate, while the state G_g is roughly 60 cm^{-1} above. Most of the vibronic structure observed in emission and in excitation spectra is due to false origins borrowing their intensity from higher T_{1u} states and to combination bands with one quantum of $h_g(1)$ and $a_g(2)$ modes. Almost all the bands of the excitation spectrum taken in the supersonic beam have been assigned in this review on the basis of calculated intensities. For one of these bands, namely the band at 1011 cm^{-1} above the S_1 origin, a simple assignment to one of the three lowest singlet states does not seems plausible. We propose tentatively that it draws its intensity from the G_g–T_{2g} pseudo-JT interaction induced by the $h_g(1)$ mode or, as an alternative, that it is associated to a fourth state, H_g, with the electronic origin 296 cm^{-1} above S_1.

It is surprising that no clear evidence of splitting of the JT-active modes and of pseudo-JT interactions has emerged in the highly resolved spectra so far available.

Moving from C_{60} to C_{70}, the molecular symmetry is lowered and the degeneracy of electronic states decreases. This fact leads to an increase in the density of electronic states and in the relative number of states with allowed spectroscopic transitions. As a consequence, for C_{70} both symmetry forbidden and allowed states are found among the lowest singlet states. In particular, the S_1 state is forbidden, while S_2, only 170 cm^{-1} above, is allowed. This leads to the observation of multiple emission, which is rather unusual for organic molecules. A detailed analysis of the vibronic structure of the excitation spectrum of C_{70} becomes very complicated and has not been obtained so far.

The complications encountered in the spectral analysis of C_{70} are expected also for the many other fullerenes that do not possess the high symmetry of C_{60}.

The lowest triplet state T_1 is well separated from T_2 both in C_{60} and C_{70}. Correspondingly, the phosphorescence spectra of both fullerenes have been assigned in detail. However, the rationalization of the different triplet lifetimes of the two fullerenes is still an open problem.

In summary, the combination of high resolution spectroscopic data along with the modeling of vibronic interactions and intensities has led to a good understanding of the vibronic structure associated with the lowest electronic states of C_{60} and, although to a lesser extent, of C_{70}. Nevertheless, several questions that would require additional experimental studies (extension of the spectral range of high resolution excitation spectra) along with additional and more accurate theoretical calculations of spectroscopic parameters (energies and interactions between the lowest excited states and between states in

Table 10 Computed vibronically induced intensities for the $T_1 \longrightarrow S_0$ transition of C_{70}, from CNDO/S+CI(29 × 29) calculations, and comparison with observed bands

Symmetry	QCFF/PI[a]	B3LYP/6-31G*[b]	I[c]	Observed[d]	Observed[e]
e_1'	1641	1569	865	1565	1562
	1569	1491	190	1492	1485
	1499	1432	126	1433	1429
	1424	1416	24		
	1384	1319	163	1323	1320
	1369	1291	32		
	1245	1256	72		1248
	1201	1178	592	1177	1176
	1119	1088	604	1089	1088
	961	751	5		
	931	906	30		902
	819	828	394	798	800
	748	730	12	710	717
	711	666	90	676	681
	650	639	170	622	649
	585	573	518	580	583
	560	533	20	537	542
	498	508	28	513	
	412	416	4	419	421
	361	359	533	361	361
	327	325	40		330
e_2''	1643	1573	17		
	1551	1517	10		
	1531	1455	4		
	1460	1399	3		
	1418	1328	1		
	1358	1317	1		
	1245	1258	6		
	1142	1156	3		
	1107	1075	1		
	940	920	2		933
	867	781	1		
	820	729	155	746	748
	739	717	1		
	710	701	1		
	682	634	3		
	610	556	0		
	516	515	3		
	405	408	18	392	
	392	382	2		
	314	304	1		
a_2''	1556	1567	9		
	1389	1463	13		
	1270	1321	2		
	1217	1207	1		
	1169	1144	2		
	895	896	1		
	684	704	4		
	592	564	49		
	485	459	88	459	459
	326	318	11		
a_1''	1658	1558	16		
	1455	1348	0		
	1342	1240	0		
	1041	892	0		
	899	781	1		
	774	734	0		
	722	613	0		
	544	530	1		
	335	336	3		

[a] Computed vibrational frequencies from ref. 30. [b] Computed frequencies from ref. 73. [c] Relative values of vibronically induced intensities from CNDO/S+CI calculations. [d] From ref. 55. [e] From ref. 56.

the spectral range of the lowest T_{1u} singlet states) still remain open.

6 Acknowledgements

We are grateful to Majed Chergui for interesting discussions. We are indebted to Gustavo Scuseria for kindly providing his unpublished full set of computed vibrational frequencies of C_{70}. Financial support from MURST (Project: "Modellistica delle Proprieta' Spettroscopiche di Sistemi Molecolari Complessi" ex 60%; Project: "Dinamiche Molecolari in Sistemi di interesse Chimico" ex 40%) and from the University of Bologna (Funds for Selected Research Topics) is gratefully acknowledged.

7 References

1 H. W. Kroto, J. R. Heath, S. C. O' Brien, R. F. Curl and R. E. Smalley, C_{60}: Buckminsterfullerene, *Nature*, 1985, **318**, 162.
2 L. W. Tutt and A. Kost, Optical limiting performance of C_{60} and C_{70} solutions, *Nature*, 1992, **356**, 225.

3 A. Warshel and M. Karplus, Calculation of Ground and Excited State Potential Surfaces of Conjugated Molecules. Formulation and Parametrization, *J. Am. Chem. Soc.*, 1972, **94**, 5612.
4 J. Del Bene and H. H. Jaffe', Use of the CNDO Method in Spectroscopy, I. Benzene, Pyridine and the Diazines, *J. Chem. Phys.*, 1968, **48**, 4050.
5 F. Negri, G. Orlandi and F. Zerbetto, Interpretation of the vibrational structure of the emission and absorption spectra of C_{60}, *J. Chem. Phys.*, 1992, **97**, 6496.
6 A. Sassara, G. Zerza, M. Chergui, F. Negri and G. Orlandi, The visible emission and absorption spectrum of C_{60}, *J. Chem. Phys.*, 1997, **107**, 8731.
7 C. Cepek, A. Goldoni, S. Modesti, F. Negri, G. Orlandi and F. Zerbetto, The EEL spectrum of the triplet exciton of C_{60} and the theoretical analysis of its vibronic structure, *Chem. Phys. Lett.*, 1996, **250**, 537.
8 C. A. Masmanidis, H. H. Jaffe' and R. L. Ellis, Spin-Orbit Coupling in Organic Molecules, *J. Phys. Chem.*, 1975, **79**, 19.
9 (*a*) H. W. Kroto, The stability of fullerenes C_n, with n = 24, 28, 32, 36, 50, 60 and 70, *Nature*, 1987, **329**, 529; (*b*) T. G. Schmalz, W. A. Seitz, D. G. Klein and G. E. Hite, Elemental Carbon Cages, *J. Am. Chem. Soc.*, 1988, **110**, 1113; (*c*) S. J. Austin, P. W. Fowler, D. E. Manolopoulos, F. Zerbetto and G. Orlandi, Structural motifs and the stability of Fullerenes, *J. Phys. Chem.*, 1995, **99**, 8076.
10 K. Hedberg, L. Hedberg, D. S. Bethune, C. A. Brown, M. de Vries, H. C. Dorn and R. D. Johnson, Bond lengths in free molecules of Buckminsterfullerene C_{60} from gas phase Electron Diffraction, *Science*, 1991, **254**, 410.
11 L. J. Terminello, D. K. Shuh, F. J. Himpel, D. A. Lapiano-Smith, J. Stoehr, D. S. Bethune and J. Meijer, Unfilled orbitals of C_{60} and C_{70} from carbon K-shell X-ray absorption fine structure, *Chem. Phys. Lett.*, 1991, **182**, 491.
12 X.-B. Wang, C.-F. Ding and L.-S. Wang, High resolution photoelectron spectroscopy of C_{60}^-, *J. Chem. Phys.*, 1999, **110**, 8217.
13 J. H. Weaver, J. L. Martins, T. Komeda, Y. Chen, T. R. Ohno, G. H. Kroll, N. Troullier, R. Haufler and R. E. Smalley, Electronic structure of solid C_{60} – Experiment and theory, *Phys. Rev. Lett.*, 1991, **66**, 1741.
14 P. A. Limbach, P. F. Crain and P. F. McCloskey, Observation of doubly charged, gas phase fullerene anions C_{60}^{2-} and C_{70}^{2-}, *J. Am. Chem. Soc.*, 1991, **113**, 6795.
15 F. Negri, G. Orlandi and F. Zerbetto, Quantum-chemical investigation of Franck–Condon, Jahn–Teller activity in the electronic spectra of Buckminsterfullerene, *Chem. Phys. Lett.*, 1988, **144**, 31.
16 (*a*) I. Laszlo and L. Udvardi, On the geometrical structure and UV spectrum of the truncated icosahedral C_{60} molecule, *Chem. Phys. Lett.*, 1987, **136**, 418; (*b*) I. Laszlo and L. Udvardi, A study of the UV spectrum of the truncated icosahedral C_{60} molecule, *J. Mol. Struct.*, 1989, **183**, 271.
17 (*a*) M. Braga, S. Larsson, A. Rosén and A. Volosov, Electronic transitions in C_{60} – On the origin of the strong interstellar absorption at 217 nm, *Astron. Astrophys.*, 1991, **245**, 232; (*b*) S. Larsson, A. Rosén and A. Volosov, Optical spectrum of the icosahedral C_{60} – "Follene-60", *Chem. Phys. Lett.*, 1987, **137**, 501.
18 R. Bauernschmitt, R. Ahlrichs, F. H. Hennrich and M. M. Kappes, Experiment versus Time Dependent Density Functional Theory Prediction of Fullerene Electronic Absorption, *J. Am. Chem. Soc.*, 1998, **120**, 5052.
19 (*a*) W. Kraetschmer, K. Fostiroupolos and D. R. Huffman, The infrared and ultraviolet absorption spectra of laboratory-produced carbon dust: evidence for the presence of the C_{60} molecule, *Chem. Phys. Lett.*, 1990, **170**, 167; (*b*) J. P. Hare, H. W. Kroto and R. Taylor, Preparation and UV/visible spectra of fullerenes C_{60} and C_{70}, *Chem. Phys. Lett.*, 1991, **177**, 394.
20 S. Leach, M. Vervloet, A. Desprès, E. Breheret, J. P. Hare, T. J. Dennis, H. W. Kroto, R. Taylor and D. R. M. Walton, Electronic Spectra and Transitions in C_{60}, *Chem. Phys.*, 1992, **160**, 451.
21 A. A. Lucas, G. Gesterblum, J. J. Pireaux, P. A. Thiry, R. Caudano, J. P. Vigneron and Ph. Lambin, Elementary excitation of C_{60} from the far infrared to the far vacuum UV, studied by high resolution Electron Energy Loss Spectroscopy, *Phys. Rev.*, 1992, **45**, 13694.
22 R. Abouaf, J. Pommier and S. Cvejanovic, Electron Impact on free C_{60}. Excited states below 10 eV, *Chem. Phys. Lett.*, 1993, **213**, 503.
23 R. E. Haufler, Y. Chai, L. P. F. Chibante, M. R. Froelich, R. B. Weisman, R. F. Curl and R. E. Smalley, Cold molecular beam electronic spectrum of C_{60} and C_{70}, *J. Chem. Phys.*, 1991, **95**, 2197.
24 J. D. Close, F. Federmann, K. Hoffmann and N. Quaas, Absorption Spectroscopy of C_{60} molecules isolated in helium droplets, *Chem. Phys. Lett.*, 1997, **276**, 393.
25 X. L. R. Dauw, M. V. Bronsveld, A. Kruger, J. B. M. Warntjes, M. R. Witjes and E. J. J. Groenen, On the singlet excited states of C_{60} and C_{70}, *J. Chem. Phys.*, 1998, **109**, 9332.
26 (*a*) A. Sassara, G. Zerza, V. Ciulin, J. D. Ganière, B. Deveaud and M. Chergui, Picosecond studies of the intramolecular relaxation processes in isolated C_{60} and C_{70} molecules, *J. Chem. Phys.*, 1999, **111**, 689; (*b*) A. Sassara, G. Zerza, V. Ciulin, M. T. Portella-Oberli, J. D. Ganière, B. Deveaud and M. Chergui, Picosecond and femtosecond studies of the energy redistribution in matrix-isolated C_{60} molecules, *J. Lumin.*, 1999, **83/84**, 29.
27 A. Sassara, G. Zerza, M. Chergui and S. Leach, Absorption wavelengths and bandwidths for interstellar searches of C_{60} in the 2400–4100 Å region, *Astron. J. Suppl. Series*, 2001, **135**, 263.
28 Z. Gasyna, P. N. Schatz, J. P. Hare, T. J. Dennis, H. W. Kroto, R. Taylor and D. R. M. Walton, The magnetic circular dichroism and absorption spectra of C_{60} isolated in Ar matrices, *Chem. Phys. Lett.*, 1991, **183**, 283.
29 F. Negri, G. Orlandi and F. Zerbetto, New assignments in the 600 nm band region of C_{60}: the origins of the T_{1g} and G_g transitions, *J. Phys. Chem.*, 1996, **100**, 10849.
30 F. Negri and G. Orlandi, The vibrational frequencies of fullerenes from an updated QCFF/PI hamiltonian, *J. Phys. B: At., Mol. Opt. Phys.*, 1996, **29**, 5049.
31 V. Schettino, P. R. Salvi, R. Bini and G. Cardini, On the vibrational assignment of fullerene C_{60}, *J. Chem. Phys.*, 1994, **101**, 11079.
32 Y. Wang, Photophysical properties of fullerenes and fullerene/N,N-diethylaniline charge transfer complexes, *J. Phys. Chem.*, 1992, **96**, 764.
33 D. J. van den Heuvel, G. J. B. van den Berg, E. J. J. Groenen, J. Schmidt, I. Hollemann and G. Meijer, Lowest Excited Singlet State of C_{60}: A Vibronic Analysis of the Fluorescence, *J. Phys. Chem.*, 1995, **99**, 11644.
34 W.-C. Hung, C.-D. Ho, C.-P Liu and Y.-P. Lee, Laser-Induced Fluorescence and Phosphorescence of C_{60} Isolated in Solid Ne, *J. Phys. Chem.*, 1996, **100**, 3927.
35 A. Sassara, G. Zerza and M. Chergui, Fluorescence spectra of isolated C_{60} molecules in neon and argon matrices: assignment of the lowest emitting states, *J. Phys. B: At., Mol. Opt. Phys.*, 1996, **29**, 4997.
36 J. H. Rice, R. Aures, J.-P. Galaup and S. Leach, Fluorescence Spectroscopy of C_{60} in toluene solutions at 5 K, *Chem. Phys. Lett.*, 2001, **263**, 401.
37 D. J. van den Heuvel, I. Y. Chan, E. J. J. Groenen, M. Matshushita, J. Schmidt and G. Meijer, On the fluorescence of crystalline C_{60} at 1.2 K, *Chem. Phys. Lett.*, 1995, **233**, 284.
38 M. Chergui, Medium effects on the spectroscopy and intermolecular energy redistribution of C_{60} in cryogenic matrices, *Low Temp. Phys.*, 2000, **26**, 632.
39 T. W. Ebbesen, K. Tanigaki and S. Kuroshima, Excited-state properties of C_{60}, *Chem. Phys. Lett.*, 1991, **181**, 501.
40 (*a*) J. W. Arbogast, A. P. Darmanyan, C. S. Foote, Y. Rubin, F. Diederich, M. M. Alvarez, S. J. Anz and R. L. Whetten, Photophysical Properties of C_{60}, *J. Phys. Chem.*, 1991, **95**, 11; (*b*) L. Biczok, H. Linschitz and R. I. Walter, Exctinction co-efficients of C_{60} triplet and anion radical, and one-electron reduction of the triplet by aromatic donors, *Chem. Phys. Lett.*, 1992, **195**, 339.
41 K. Hansen, R. Mueller, P. Brockhaus, E. E. B. Campbell and I. V. Hertel, Resonant two-photon ionization spectroscopy of C_{60}, *Z. Phys. D: At. Mol. Clusters*, 1997, **42**, 153.
42 M. Chergui, personal communication.
43 (*a*) R. Signorini, M. Meneghetti, R. Bozio, M. Maggini, G. Scorrano, M. Prato, G. Brusatin, P. Innocenzi and M. Guglielmi, Optical limiting and non linear optical properties of fullerene derivatives embedded in hybrid sol-gel glasses, *Carbon*, 2000, **38**, 1653; (*b*) M. Maggini, C. De Faveri, G. Scorrano, M. Prato, G. Brusatin, M. Guglielmi, R. Signorini, M. Meneghetti and R. Bozio, Synthesis and optical limiting behavior of hybrid inorganic-organic materials from the sol-gel processing of organofullerenes, *Chem. Eur. J.*, 1999, **5**, 2501.
44 M. R. Wasielewski, M. P. O'Neil, K. R. Lykke, M. J. Pellin and D. M. Gruen, Triplet states of fullerenes C_{60} and C_{70} – Electron paramagnetic resonance spectra, photophysics and electronic structure, *J. Am. Chem. Soc.*, 1991, **113**, 2774.
45 D. J. van den Heuvel, I. Y. Chan, E. J. J. Groenen, J. Schmidt and G. Meijer, Phosphorescence of C_{60} at 1.2 K, *Chem. Phys. Lett.*, 1994, **231**, 111.
46 R. V. Bensasson, T. Hill, C. Lambert, E. J. Land, S. Leach and T. J. Truscott, Pulse radiolysis study of buckminsterfullerene in benzene solution. Assignment of the C_{60} triplet-triplet absorption spectrum, *Chem. Phys. Lett.*, 1993, **201**, 326.

47 Y. Kaiji, T. Nakagawa, S. Suzuki, Y. Achiba, K. Obi and K. Shibuya, Transient absorption, lifetime and relaxation of C_{60} in the triplet state, *Chem. Phys. Lett.*, 1991, **181**, 100.
48 M. G. Giuffreda, F. Negri and G. Orlandi, Quantum-Chemical Modeling and Analysis of the Vibrational Structure in the Phosphorescence Spectrum of C_{60}, *J. Phys. Chem. A*, 2001, **105**, 9123.
49 Y. Zeng, L. Biczok and H. Linschitz, External Heavy Atom Induced Phosphorescence Emission of Fullerenes: the Energy of Triplet C_{60}, *J. Phys. Chem.*, 1992, **96**, 5237.
50 A. Sassara, G. Zerza and M. Chergui, Phosphorescence of C_{60} in rare gas matrices, *Chem. Phys. Lett.*, 1996, **261**, 213.
51 X. L. R. Dauw, PhD thesis, Leiden University, 2000.
52 A. Kupperman, W. M. Flicker and O. A. Mosher, Electronic Spectroscopy of Polyatomic Molecules by Low-Energy, Variable-Angle Electron Impact, *Chem. Rev.*, 1979, **79**, 77.
53 K. Palewska, J. Sworakowski, H. Chojnacki, E. C. Meister and U. P. Wild, A Photoluminescence Study of Fullerenes: Total Luminescence Spectroscopy of C_{60} and C_{70}, *J. Phys. Chem.*, 1993, **97**, 12167.
54 F. Negri and G. Orlandi, Vibronic structure in the multiple state fluorescence spectrum of C_{70}: a theoretical investigation, *J. Chem. Phys.*, 1998, **108**, 9675.
55 J. B. M. Warntjes, I. Holleman, G. Meijer and E. J. J. Groenen, Photoluminescence of Molecular C_{70} at 1.5 K. On the nature of the lowest excited states, *Chem. Phys. Lett.*, 1996, **261**, 495.
56 A. Sassara, G. Zerza and M. Chergui, Assignment of the lowest excited states of C_{70} and evidence for fluorescence from the S_2 state, *J. Phys. Chem. A*, 1998, **102**, 3072.
57 J. W. Arbogast and C. S. Foote, Photophysical properties of C_{70}, *J. Am. Chem. Soc.*, 1991, **113**, 8886.
58 S. M. Argentine, A. H. Francis, C.-C. Chen, C. M. Lieber and J. S. Siegel, Unusual Photoluminescence Behavior of C_{70}, *J. Phys. Chem.*, 1994, **98**, 7350.
59 S. M. Argentine, K. T. Kotz and A. H. Francis, Temperature, Solvent Effects on the Luminescence Spectrum of C_{70}: Assignment of the Lowest Singlet and Triplet States, *J. Am. Chem. Soc.*, 1995, **117**, 62.
60 (*a*) B. S. Razbirin, A. N. Starukhin, A. V. Chugreev, Y. S. Grushko and S. N. Kolesnik, Observation of fine structure in the optical spectrum of the fullerene C_{70} in a crystalline matrix, *JETP Lett.*, 1994, **60**, 451; (*b*) A. N. Starukhin, B. S. Razbirin, A. V. Chugreev, D. K. Nelson, Y. S. Grushko, S. N. Kolesnik, J. M. Hvam, D. Birkedal, K. Litvinenko, C. Spiegelberg, J. Zeman and G. Martinez, High-resolution spectroscopy of matrix-isolated fullerene molecules, *J. Lumin.*, 1997, **72–74**, 457.
61 F. Negri and M. Z. Zgierski, On the vibronic structure of the $S_0 \longrightarrow S_1$ transitions in azulene, *J. Chem. Phys.*, 1993, **99**, 4318.
62 J. Feng, J. Li, Z. Li and M. Zerner, Quantum Chemical calculations of Buckminsterfullerene and related structures. 2. The electronic structure and spectra of some C_n and C_nCa^{2+} cages, *Int. J. Quantum Chem.*, 1991, **39**, 331.
63 F. Negri, G. Orlandi and F. Zerbetto, QCFF/PI vibrational frequencies of some spherical carbon clusters, *J. Am. Chem. Soc.*, 1991, **113**, 6037.
64 F. Negri and G. Orlandi, The electronic spectroscopy of C_{60} and C_{70}: A semiempirical study, *Z. Phys. Chem.*, 1997, **200**, 85.
65 A. Fedorov, M. N. Berberan-Santos, J. P. Lefevre and B. Valeur, Picosecond time-resolved and steady-state studies of polarization of the fluorescence of C_{60} and C_{70}, *Chem. Phys. Lett.*, 1997, **267**, 467.
66 F. Negri and M. Z. Zgierski, Vibronic structure of the emission spectra from single vibronic levels of the S_1 manifold in naphthalene: Theoretical simulation, *J. Chem. Phys.*, 1996, **104**, 3486.
67 F. Negri and M. Z. Zgierski, Theoretical analysis of the vibronic structure of the zero-kinetic-energy photoelectron spectra from single vibronic levels of the S_1 state manifold of naphthalene, *J. Chem. Phys.*, 1997, **107**, 4827.
68 J. Fulara, M. Jakobi and J. P. Maier, Electronic spectra of the C_{70} molecule and C_{70}^+, C_{70}^- ions in neon matrices, *Chem. Phys. Lett.*, 1993, **206**, 203.
69 F. Negri, G. Orlandi, F. Zerbetto and M. Z. Zgierski, Quantum chemical and vibronic analysis of the $1^2B_2 \leftrightarrow 1^2A_2$, 2^2B_2 transition in benzyl-h_7 and benzyl-d_7 radicals, *J. Chem. Phys.*, 1990, **93**, 600.
70 R. V. Bensasson, T. Hill, C. Lambert, E. J. Land, S. Leach and T. G. Truscott, Triplet state absorption studies of C_{70} in benzene solution, *Chem. Phys. Lett.*, 1993, **206**, 197.
71 (*a*) X. L. R. Dauw, O. G. Poluektov, J. B. M. Warntjes, M. V. Bronsveld and E. J. J. Groenen, Triplet state dynamics of C_{70}, *J. Phys. Chem. A*, 1998, **102**, 3078; (*b*) M. V. Bronsveld, X. L. R. Dauw and E. J. J. Groenen, The triplet state of C_{70}. A zero-field study, *Chem. Phys. Lett.*, 1998, **293**, 528.
72 F. Negri and G. Orlandi, On the analysis of the phosphorescence spectrum of C_{70}, *J. Phys. B: At., Mol. Opt. Phys.*, 1996, **29**, 5077.
73 (*a*) R. E. Stratmann, G. E. Scuseria and M. J. Frisch, Density Functional study of the infrared vibrational study of C_{70}, *J. Raman Spectrosc.*, 1998, **29**, 483; (*b*) G. E. Scuseria, personal communications.